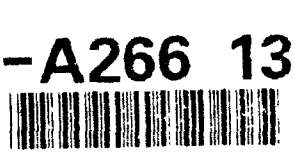

OFFICE OF NAVAL RESEARCH

Contract No. N00014-91-J-1409

Technical Report No. 140

Real-Space Formation and Dissipation Dynamics of Hexagonal Reconstruction on Au(100) in Aqueous Media as Explored by Potentiodynamic Scanning Tunneling Microscopy

by

Xiaoping Gao, Gregory J. Edens, Antoinette Hamelin, and Michael J. Weaver

Prepared for Publication

in

Surface Science

Department of Chemistry

Purdue University

West Lafayette, IN 47907-1393

April 1993

Abstract

The electrode potential-induced formation and dissipation dynamics of the hexagonal ("hex") reconstruction on ordered Au(100) in perchloric and sulfuric acid electrolytes has been studied by means of in-situ scanning tunneling microscopy (STM). The real-space/real-time evolution of surface structures associated with the potential-dependent hex $\leftrightarrows$ (1 × 1) phase transition was examined on timescales down to ca 1 s by acquiring STM images during appropriate potential sweeps and steps (dubbed here "potentiodynamic STM"). Extensive hex domains can be formed by slow cooling following flame annealing and/or by holding the potential at values significantly below the potential of zero charge for the (1 × 1) surface. The sharp removal of the reconstruction seen voltammetrically, during positive-going potential sweeps, is accompanied by rapid (< 1 s) formation of arrays of ordered (1 × 1) clusters, created from the release of the ca 24% additional gold atoms utilized in the (5 × 27) and related hex structures compared with the (1 × 1) substrate. These clusters are significantly, twofold, larger (ca 4–6 nm) when formed in sulfuric acid electrolyte, due probably to an enhanced surface mobility in the presence of adsorbed sulfate. The reverse (1 × 1) → hex transition at negative electrode charges is markedly slower. The hex domains appear initially as long thin (few atom-wide) strands, formed on (1 × 1) terraces by adatom diffusion primarily from cluster sites. This mechanism is augmented close to terrace edges by a "wavefront-like" motion of atomic rows. Further development of the hex domains occurs partly by aggregation of very thin hex strings, but primarily by a uniform broadening of thicker strands. The considerable prospects for utilizing potentiodynamic STM to explore local nanoscale processes associated with reconstruction and other potential-induced phase transitions is noted in the light of these findings.

INTRODUCTION

Reconstruction of metal surfaces, whereby at least the top layer of atoms rearrange to form ordered structures that differ from that expected from a simple termination of the bulk-phase crystal lattice, is an extremely well characterized phenomenon for surfaces in vacuum environments.[1] While much less is known concerning surface reconstruction in electrochemical systems, a detailed picture is emerging for low-index gold surfaces in aqueous media.[2] Interest in these systems stems in part from the occurrence of potential-dependent reconstruction. For all three low-index faces in weakly adsorbing electrolytes such as perchloric acid, the (1 × 1) (i.e. unreconstructed) surfaces are found to be stable over most positive electrode charge densities, yet reconstruction is prevalent at negative charges. Interconversion between the (1 × 1) and reconstructed forms of these surfaces can indeed be induced by suitable alterations in electrode potential, thereby offering a valuable degree of control of the reconstruction stability and dynamics which is not available for the more well-studied metal-vacuum interfaces.

Experimental evidence for this phenomenon was garnered originally from conventional electrochemical measurements.[3] More persuasive information, however, has become available recently from in-situ microscopic methods, especially electroreflectance,[4] second harmonic generation,[5] and most directly from X-ray diffraction[6,7] and scanning tunneling microscopy.[8-11] The last technique, in particular, can now yield detailed real-space structural information with true atomic resolution. This enables hitherto unattainable information concerning the spatial atomic arrangements of the metal substrate as well as adsorbed species to be extracted for in-situ electrochemical interfaces at a level of sophistication which is on a par with, or even beyond, that achieved for metal-vacuum interfaces.

Of the three low-index faces, Au(100) has come under particular scrutiny.[4-6,8] In weakly adsorbing electrolytes such as perchloric acid, the square-planar bulk-termination structure is prevalent only at potentials significantly above the potential of zero charge, E_{pzc}; at negative electrode charges the (1 × 1) surface is unstable with respect to formation of a near-hexagonal metal overlayer.[8] This "hex" reconstruction occurs on clean Au(100) in vacuum, and has been subjected to a number of detailed structural studies, primarily using low-energy electron diffraction (LEED).[12] The electrochemically generated hex reconstruction exhibits closely similar structures, featuring an approximate (5 × 27) unit cell, although a myriad of structural mutations are evident upon detailed scrutiny with in-situ STM.[8b] At least in perchloric acid, the electrode potential- (or charge-) induced production of the "hex" phase is slow, typically requiring 10-20 mins for extensive formation.[8] Dissipation of the reconstruction, however, can be driven to occur over shorter timescales, down to 0.01 s, depending on the applied potentiodynamic conditions (potential sweeps, steps).[13]

These properties offer some intriguing opportunities by which in-situ STM can be utilized to follow the evolution of real-space structural changes required for the occurrence of surface reconstruction. Some initial observations of this type have been reported recently from our laboratory.[8b,d] Most simply, temporal sequencies of STM images following suitable potential perturbations can allow relatively slow ($\gtrsim$ 10-20 s) alterations in surface structure associated with the formation and dissipation of the reconstruction to be probed. In addition, however, much faster structural changes can also be followed by applying suitable electrode potential perturbations *during* the acquisition of a given STM image. We have recently utilized this latter tactic, dubbed here "potentiodynamic STM," to follow subtle potential-induced changes in electrochemical adlayer structure

and to obtain unusually accurate adsorbate-substrate symmetries and registries.[9c,14,15]

In the present paper, we present and discuss detailed STM data gathered along these lines for Au(100) in aqueous acidic electrolytes with the central objective of elucidating the nature of the nanoscale mass transport of metal atoms associated with the potential-induced formation and dissipation of the surface reconstruction. The perchloric and sulfuric acid electrolytes used here enable at least the reconstruction formation dynamics to be examined in the absence of anion specific adsorption. We discuss elsewhere a related study undertaken in strongly chemisorbing iodide media, where adsorption plays a dominant role in the reconstruction dynamics.[16] Taken together, the results illustrate how potentiodynamic STM can provide substantial, yet heretofore untapped, insight into the atomic motions responsible for such substrate phase transitions on ordered metal surfaces.

EXPERIMENTAL SECTION

The experimental STM procedures were largely as described elsewhere.[8,9] The microscope is a Nanoscope II (Digital Instruments) with a bipotentiostat for in-situ electrochemical STM. The STM tips were 0.01 in. tungsten wire etched electrochemically in 1 M KOH. The STM images were obtained using the "constant current" mode, unless noted otherwise. The faradaic leakage current was typically < 0.1 nA. Three methods were employed for insulating the tungsten wire so to minimize this current. The approach utilized most extensively in our laboratory (and earlier by the Schardt group at Purdue) involves painting the wire with clear nail varnish ("Wet 'n Wild", Pavion Ltd.). While this method enables excellent atomic-resolution images to be obtained most reproducibly, some substrate surface contamination is sometimes evident in gold by distortions in

the voltammetry at higher potentials, above ca 0.5 V vs SCE. For this reason, we now also commonly employ two alternative tip-coating methods where the minimization of surface contamination is deemed important. The first, and conventional, approach involves briefly dipping the tip in hot Apiezon wax. The second, and preferred, method entails the use of thermosetting polyethylene plastic as dispensed by a commercial (Sears) "glue gun." The advantage of this tactic is that a thin uniform plastic coating can be applied up to (but not encompassing) the tip point, which yields contaminant-free voltammograms within the STM cell over the long periods (several hours) that are often desired.

The Au(100) crystal (hemisphere, 5 mm diameter) was manufactured at LEI-CNRS. It was flame annealed, cooled in air and/or ultrapure water (vide infra), and transferred to the STM cell protected by a drop of water. The STM electrochemical cell, machined from Teflon, is secured to the gold substrate base by a pair of set screws. The cell holder, machined from Kel-F, contains the counter and reference electrode connections. The former electrode was gold, and the latter, quasi-reference, electrode was an electrooxidized gold wire except with the iodide electrolytes where a platinum wire was used instead. All electrode potentials quoted here, however, are converted to the saturated calomel electrode (SCE) scale.

RESULTS

Initial state of Au(100) surface

As a prerequisite to the examination of potential-induced changes in Au(100) surface structure, it is clearly desirable to prepare the surface in a reproducible as well as well-ordered state prior to its insertion in the electrochemical STM cell. A common procedure, undertaken by Hamelin[3] and also by Kolb et al,[4] entails annealing by heating to redness in an oxy-gas flame,

cooling at least partly in ultrapure water so to maintain surface cleanliness, followed by immediate transfer to the electrochemical cell. At least two sources of variance in the resulting Au(100) electrochemical surface structure can be anticipated, resulting from atomic structural differences associated broadly with alterations in (a) the annealing-cooling procedure, and (b) the electrode potentials applied in the electrochemical cell.

While (b) is of greater interest here, the possible variability of (a) clearly should be addressed. This can be achieved in part by means of STM measurements undertaken following both replicate, and deliberately altered, annealing-cooling procedures. We recently reported some preliminary measurements along these lines.[8c] Most importantly, marked differences are seen between annealed Au(100) surfaces that undergo cooling predominantly in argon or air (Method I), and those that are transferred to water rapidly (say within ca 2-5s) after withdrawal from the flame (Method II). Specifically, the former procedure yields surfaces featuring ordered domains of chiefly reconstructed Au(100). Examples of STM images for a large (ca 100 nm square) region of a Au(100) surface prepared using Method I are given in Figs. 1A and B. (The constant-height image B was recorded at 0.2 V vs SCE in 0.1 M $HClO_4$, but concordant results could also be obtained in air, as shown in A.) Clearly evident are corrugated strands, which in B run roughly parallel to the substrate atomic rows in both possible directions (90° to each other), and in A preferentially in one direction. These corrugations, which are characteristic of Au(100) surface reconstruction, arise from the periodic undulations in the binding site of the hexagonal top layer of gold atoms on the underlying square-planar substrate.[8b] (Atomic-resolution images show that six gold atoms are hexagonally compressed within the distance (14.5 Å) occupied by five atoms along the (100) direction of the underlying substrate.)

In contrast, however, Au(100) surfaces prepared by Method II tend to yield well-ordered domains having a predominantly *unreconstructed* [i.e. (1 × 1)] structure.[8c] The latter circumstance was most commonly encountered in our laboratories (Purdue and CNRS), since rapid cooling in ultrapure water has been preferred in order to minimize the risk of surface contamination.[8c] Nevertheless, STM measurements undertaken at Purdue involving systematic variations in the Au(100) crystal cooling procedure have recently convinced us of the sensitivity of the ensuing surface structure to the particular protocol followed.

At least a qualitative rationalization of the observed differences in the initial structure of Au(100) surfaces prepared by Methods I and II can be offered. The former procedure, especially in its extreme form where the cooling is undertaken entirely in the gas phase, yields the same reconstructed structure as seen for Au(100) surfaces annealed under vacuum conditions. This is unsurprising since clean Au(100) spontaneously reconstructs at elevated temperatures, the hex phase being thermodynamically more stable than the (1 × 1) surface structure.[12] At first sight, one might expect that cooling predominantly in water (Method II) would yield similar results, since water adsorbs only very weakly on gold. However, we suspect that a key element lies in the usual presence of dissolved oxygen. Once the crystal is immersed in the water, the propensity for oxygen to reduce (to peroxide) on gold will charge the surface positive and thereby raise the surface potential.[17] While the detailed kinetics and hence the resultant shifts in electrode potential will inevitably be sensitive to the temperature, pH, etc., given the elevated temperatures involved one might expect that the potential will acquire values substantially positive of E_{pzc}, perhaps above 0.5–0.6 V vs SCE. As detailed below, this condition yields a stabilization of the (1 × 1) with respect to the hex structure, so that the latter rapidly rearranges to the former. Some support for this notion was

obtained from experiments in which the crystal was cooled instead in deoxygenated water, which tended to yield partly reconstructed surfaces. Ross and coworkers[6b] report that a largely (1 × 1) Au(100) surface is formed by flame annealing and subsequent cooling in hydrogen to about 400 K, followed by contact with water. Presumably the last step is sufficient to lift the reconstruction.

These factors may offer a partial reconciliation of the differing initial voltammetric behavior reported earlier for Au(100) by Kolb et al[4] and Hamelin.[3,8c] The former workers maintain that their Au(100) surface is initially reconstructed, which can be lifted by sweeping the electrode potential to about 0.6 V and 0.4 V in perchloric and sulfuric acid media, respectively.[4c] Supporting their contention is a sharp voltammetric "spike," located at these potentials, which turns out to arise from the lifting of the reconstruction at this point (vide infra).[4] Similar voltammetric features, although typically much less pronounced, are discernable in initial positive-going potential sweeps reported by Hamelin in these media.[3b] This is consistent with the presence of largely (1 × 1), rather than hex, domains when using the Method II annealing procedure.

Nonetheless, it is crucial to recognize that extensive reconstruction can be induced on Au(100) surfaces prepared in the latter fashion by holding the potential at suitably negative values, below ca −0.2 V vs SCE, for 10–20 mins. This *potential*-induced reconstruction is seen most directly by means of in-situ STM,[8] and is considered further below. The voltammetric consequencies of the phenomenon are also instructive. As an illustration, Fig. 2 contains a trio of voltammograms obtained for Au(100) in 10 mM $HClO_4$. The solid curve shows an initially positive-going voltammogram starting from 0 V at 50 mV s^{-1}, for a surface prepared by Method I. The pronounced current-potential spike (labeled C_p) at about 0.6 V, corresponding to the lifting of the thermally induced

reconstruction, is clearly evident. The positive-going dashed voltammogram was obtained for a surface prepared by Method II, but after holding the potential at -0.35 V for 10 mins. The presence of a similar voltammetric spike, albeit at a slightly lower potential, is clearly seen, indicating the extensive reconstruction formed in this case largely by electrochemical means. In contrast, voltammograms obtained following potential excursions above 0.6-0.7 V, and without subsequent holding at negative potentials, do not show this voltammetric feature. An example is the dotted voltammogram in Fig. 2. A noteworthy property of this last trace is the current-potential minimum seen close to 0 V, appearing for both the positive- and negative-going sweeps in symmetric fashion. This minimum, which deepens as the electrolyte concentration is decreased, corresponds to E_{pzc} for the (1 × 1) surface.[8c,d]

Reconstruction Lifting as Probed by Potentiodynamic STM

As already mentioned, the observation of distinct voltammetric features associated with such surface phase transitions offers interesting opportunities by which the associated alterations in real-space structure can be monitored by combined voltammetric-STM measurements. Examples of such "potentiodynamic" STM data gathered during positive-going potential sweeps similar to those in Fig. 2 are shown in Figs. 3A-D. The first three "constant-height" images (Figs. 3A-C) were recorded for a fresh Au(100) surface in 0.1 M $HClO_4$, prepared by Method I, during an initial positive-going sweep from -0.2 V at 10 mV s^{-1}. The tip potential was held at ca 0 V vs. SCE. Image A was recorded in about 25 s while the substrate potential was swept from ca 0.05 to 0.3 V vs SCE, the tip being rastered from the top to bottom of the screen image as shown. As a consequence, the y-axis of Fig. 3A can be considered to be a linear scale of electrode potential as well as real-space and time.

In such a low potential region, the thermally produced reconstruction is stable, so that this potentiodynamic STM image exhibits dense patches of the characteristic corrugated strands, similar to those seen in images obtained under conventional fixed-potential conditions (e.g. Fig 1B). Dramatically different STM behavior is seen, however, once the electrode potential traverses the region where the voltammetric peak C_p (Fig. 2) is located. Figure 3B is such an image, obtained following A, but while the substrate potential is swept between 0.59 and 0.75 V. Again, the tip was rastered from top to bottom so that the y-axis constitutes a downward-increasing potential scale starting at 0.59 V. In contrast to A (and an additional image, not shown, acquired between A and B), the densely packed corrugated strands of hex reconstruction are largely removed close to the top of the image (i.e. at about 0.6 V), being replaced by an array of clusters dotted over the substrate. Note that the clusters are clearly identified as protrusions above the (1 × 1) substrate background from the brighter appearance of the right-hand edge; this arises from the higher tunneling current obtained at these points in the "constant-height" images as the tip is scanned from right to left. [Also, while not observable in such large-area images, the ordered (1 × 1) (i.e. square-planar) atomic nature of the surrounding substrate is clearly evident in higher-magnification STM data.[8]] Of interest is a hex domain seen towards the top left-hand corner, which is apparently "trapped" by newly formed clusters that surround it. All traces of the hex domains are nonetheless removed by the middle of the image, corresponding to about 0.64 V. These findings, which were typically obtained during a number of replicate potentiodynamic STM sequencies, are therefore in harmony with the voltammetric data, which indicate that the hex reconstruction is lifted over a ca 30-50 mV region close to 0.6 V (Fig. 2). Figure 3C shows the STM image taken immediately after B. Comparison between B and C confirms the complete removal of the hex

phase. Moreover, many of the small gold clusters created initially upon lifting the reconstruction have undergone aggregation.

Closely similar findings are obtained by means of potentiodynamic STM for the removal of hex reconstruction formed *electrochemically* at negative potentials. Figure 3D is such an example, again obtained during a positive-going potential sweep at 10 mV s^{-1}, but now by rastering the tip upwards, so that the y-axis corresponds to a vertically increasing potential scale from 0.45 to 0.65 V. The majority of the hex corrugated strands are seen to be sharply dissipated at about 0.6 V, again yielding an array of gold clusters towards higher potentials. Once formed, and following some initial aggregation, the clusters are stable over substantial time periods (at least 30 mins) within the potential range ca 0.1–0.85 V in 0.1 M $HClO_4$ (vide infra). Excursions to higher potentials, where anodic oxide is formed, tends to yield substantial further coalescence into larger (50–200 Å) terrace-like features. These changes can be most readily discerned upon subsequent reduction of the oxide, at about 0.7 V during the reverse (negative-going) potential sweep.

As enunciated particularly by Kolb and coworkers,[4] the voltammetrically induced lifting of the hex Au(100) reconstruction is sensitive to the occurrence of specific adsorption in that the peak C_p occurs at lower potentials in electrolytes, such as sulfuric or hydrochloric acids, featuring stronger anion adsorption.[4b] Thus in the former electrolyte, C_p is observed at about 0.4 V. Figure 4 shows a pair of potentiodynamic STM images acquired during a 10 mV s^{-1} positive-going sweep, similar to Fig. 3 but obtained in 0.1 M H_2SO_4. The surface, prepared by Method II, was held at −0.4 V for 20 min beforehand so to generate the uniform reconstructed domains shown in Fig. 4A. This image was obtained while sweeping the potential from 0.1 to 0.3 V, the tip being rastered upwards. Figure 4B shows the next image in this sequence, the potential region

being 0.3 to 0.5 V, with the STM tip now returning in the downward direction. Once again, the hex domains are seen to be dissipated sharply during the potential sweep, being replaced by uniform cluster arrays.

However, aside from the lower potential at which the phase transition occurs, 0.4 V in 0.1 M H_2SO_4 versus 0.6 V in 0.1 M $HClO_4$, the clusters tend to be larger when formed by this means in the former electrolyte. Thus the initial cluster diameter in H_2SO_4 is ca 4–6 nm, as compared to 2–4 nm in $HClO_4$. The ensuing cluster aggregation can readily yield substantially larger clusters, even in the absence of anodic oxide formation. In most cases, the clusters appear to form monoatomic layers on the (1 × 1) substrate. This assertion, derived from the apparent z-corrugation in the STM images, is consistent with the area (ca 20%) occupied by the clusters relative to the surrounding substrate, thereby roughly matching the additional atomic density of the hex domains from which they are formed.

Potential-Induced Formation of Hex Reconstruction

Perhaps the most challenging as well as intriguing aspect of the present systems is elucidating the manner in which the ordered domains of the hex phase are formed electrochemically from the unreconstructed surface. Surface mass transport clearly plays a crucial role here since the (5 × 27) and related hex structures feature a 24% higher atomic density than the (1 × 1) Au(100) phase. A complicating feature is that it is difficult or even impractical to produce large defect-free (1 × 1) terraces in perchloric or sulfuric acid electrolytes by using the procedures described above. Thus surfaces prepared by Method I exhibit largely hex domains: while these can be lifted at positive electronic charges the resultant cluster arrays are anticipated to influence the ensuing reconstruction dynamics. Although Method II tends to yield (1 × 1) domains, also

prevalent on the surfaces are arrays of "mesas": small (5-10 nm) (100) oriented monolayer clusters.[8b] (These are probably created from the excess gold atoms freed by lifting the hex reconstruction during the water-cooling step in Method II). Nevertheless, it is of substantial interest to explore the real-space/real-time formation of the hex reconstruction induced at negative electronic charges from such largely (1 × 1) surfaces.

Figure 5A-F shows a typical sequence of STM data obtained with this objective in mind. The images show a given terrace for a Au(100) surface prepared by Method II, after the electrochemically induced reconstruction (as in Fig. 4) was lifted in 0.1 M H_2SO_4 by sweeping the electrode potential to 0.6 V. The first image, A, was acquired immediately after stepping the potential to 0 V. The array of gold clusters on the ordered (1 × 1) substrate was initially unaltered from the previous image, recorded at 0.6 V. Significant changes begin to be evident after a few minutes, as discerned in Fig. 5B, recorded 5 min after A. Several narrow (ca 15-45 Å wide) strings have now grown between some of the clusters, approximately parallel to both substrate atomic row directions. Careful comparison between A and B shows that the formation of these strings is accompanied by significant changes in the shape and size of nearby clusters. More specifically, the smallest (40-50 Å) clusters lying in the path of the strings are largely dissipated in B, and some larger clusters nearby have also receded somewhat.

Examination of images at higher (atomic-scale) magnification shows that the "strings" are composed of hexagonal close-packed gold atoms.[8b] Note that a 6-atom wide hexagonal array [i.e the unit-cell width in the (5 × 27) structure] is 14.5 Å wide (atom center-to-center; see Fig. 3 in ref. 8b), so that these strings in Fig. 5B are about 6-18 atoms (i.e. 1-3 unit cells) across. In some cases, the strands appear to be extremely narrow, down to ca 2-4 atoms wide. A number of

distinct structures can be identified, featuring different z-corrugations both across and even along the strings. Figure 6 shows a clear atomic-resolution example of one such type of narrow string, featuring a 3-atom wide, hexagonal-packed structure.

Apparent "precursor structures", formed en route to the strings evident in Fig. 5B, could sometimes also be discerned. For example, careful inspection of the area close to the cluster in the bottom right-hand corner of Fig. 5A, and the subsequent image, shows a jagged thin (ca 3 atom-wide) string of gold atoms spreading into the adjacent terrace region. Over 1-2 mins, this string becomes straighter, wider, and aligned more closely to the substrate atomic direction. (Unfortunately, half-tone reproduction of the image prints for publication renders such fine detail, seen clearly in the original STM data, no longer discernable.)

Figure 5C is an image of the same area taken 10 mins after Fig. 5B, also at 0 V. Comparison of these data show some significant changes. First, some of the strings in B, most clearly the strand towards the top left-hand corner, have become extended by "eating" part or all of clusters lying in their path. Second, new strings have appeared (see the bottom right-hand corner). Third, some lateral motion of the strings is evident, together with significant aggregation of the surviving clusters. Also commonly observed in sequences of STM images acquired under these "slow hex growth" conditions is the sudden appearance of new strings in some cases after several minutes have elapsed, in spatial regions where no previous hex formation has occurred.

More substantial as well as rapid development of the surface reconstruction is triggered by stepping the potential to lower values. Figure 5D is an image, following Fig. 5C, recorded upon altering the potential to -0.3 V. (More precisely, the potential was stepped from 0 to -0.3 V shortly after initiating

the STM scan, rastered in the downward direction.) A number of additional separate hexagonal strings appear immediately (i.e. at least within a few seconds), including some formed well away from cluster sites or trapped within areas bordered by other strands. These are typically only 3 atoms wide. Some strands are also now evident *upon*, as well as between, the remaining cluster mesas. Figures 5E and F, are taken 20 s and 5 min, respectively after completing the image in Fig. 5D. The thin strings that appeared initially in Fig. 5D have undergone only minor additional development in Fig. 5E. Nevertheless, the appearance of new strands and the broadening of existing hex regions is clearly evident in Fig. 5F. Holding the potential at, say −0.3 to −0.4 V for 20 mins or longer, yields more densely packed and ultimately uniform arrays of hex reconstructed domains.[8b] The progressively denser and broader arrays of the hexagonal strings apparently continue to grow at least partly at the expense of the cluster regions, thereby inferring that the latter provide a major source of the additional atoms required.

Indication that these atoms are supplied from additional sources, especially terrace edges, is evident from other images. An illustration of this point is provided in Figs. 7A–D, which shows a sequence of "constant height" STM images for a Au(100) surface in 0.1 M $HClO_4$ prepared by Method II, recorded at approximately 2 min intervals after altering the potential from 0.2 to −0.3 V. In addition to the mesas, a terrace edge is present, which runs diagonally from the bottom right-hand towards the top left-hand corner. In Fig. 7A, taken 2 min after stepping to −0.3 V, some reconstruction strands have become evident near and roughly parallel to the terrace edge. The following images (Figs. 7B–D) show a progressive formation of additional strings, which move apparently as a "concerted wavefront" away from the terrace edge. In addition, some smaller mesas nearby are seen to recede during this process.

Once such reconstruction has been formed, it is of interest to examine the potential range over which these hex structures are stable. Useful information along these lines can readily be obtained by holding the potential of a reconstructed surface at progressively more positive values and for varying times, and inspecting the magnitude of the voltammetric peak C_p (Fig. 2) obtained during an ensuing positive-going potential sweep. Such experiments showed that the reconstruction is stable in 0.1 M $HClO_4$ for at least 5-10 mins up to about 0.31 V, but was slowly dissipated on this timescale at 0.35-0.4 V. Figure 8 is a temporal sequence of images for a Au(100) surface at 0.4 V in 0.1 M $HClO_4$, prepared by Method II, and after forming reconstructed strands by holding at -0.4 V for 20 min. The first image was acquired almost immediately after stepping to 0.4 V, with the subsequent images recorded at ca 2 min intervals. Extensive dissipation of the reconstructed domains is seen clearly to occur by the last image (6). Interestingly, the initial dispersal of the three major reconstructed strands occurs primarily by shortening rather than narrowing the strings, but, with the latter becoming more evident in the later images.

In contrast to sulfate and especially perchlorate, iodide anions are strongly adsorbed on Au(100) and other gold surfaces, so that high and even near-saturation iodide coverages are readily formed within the polarizable potential range in aqueous media.[14,15,18] By analogy with the known effects of electron-donating adsorbates on surface reconstruction in uhv,[19] it would therefore be anticipated that the Au(100) hex reconstruction would be lifted at substantially lower potentials in iodide electrolytes than in weakly adsorbing media. This expectation turns out to be fulfilled: in addition, the chemisorbate exerts a dramatic effect upon the reconstruction dynamics. These results will be described in detail elsewhere.[16] Briefly, the hex reconstruction can be lifted

and also reformed extremely rapidly (< few sec) under potential step or sweep conditions. This phase transition is accompanied by long-range (ca 50 nm) mass transport of gold atoms, so to yield remarkably large and uniform terraces. This rapid room-temperature "annealing" effect occurs under conditions where the iodide is adsorbed extensively but in a disordered state.

DISCUSSION

Potential-Dependent Phase Equilibria

Before discussing the microscopic mechanisms responsible for the formation and removal of the hex reconstruction, it is appropriate to consider the potential-dependent driving force responsible for the overall phenomenon. Ross and D'Agostino have given an instructive analysis of the problem, based on surface tension-electrode potential (γ - E) plots for the (1 × 1) and hex phases of Au(100).[20] Most simply, the stable phase at any potential should be that exhibiting the lower surface tension, and hence free energy. The observation that the hex ⇌ (1 × 1) transition can be driven in either direction, depending on the electrode potential, indicates that the (γ - E) curves for these surface phases cross such that the hex and (1 × 1) phases exhibit smaller γ values at lower and higher potentials, respectively.[20] These authors presented γ - E plots deduced from doubly integrated capacitance-potential (C_d - E) data combined with estimated E_{pzc} values for the hex and (1 × 1) surfaces. The vertical displacement between the curves at E_{pzc}, equal to the difference in the maximum γ values for the hex and (1 × 1) phases, $\Delta\gamma_{max}$, was assumed to be 220 dynes cm^{-1}, as calculated from a tight-binding model for the clean surface.[21]

The difficulty with the analysis, as noted by Ross and D'Agostino, is that the γ - E curves calculated in this fashion for Au(100) in perchloric acid

electrolyte do not cross within the polarizable potential region, inferring that the hex phase should always be stable under these conditions. Preferential adsorption, perhaps of trace chloride, on the (1 × 1) surface was suggested as a means of accounting for the observed occurrence of the hex → (1 × 1) phase transition at moderate positive charge densities, since then the γ values for the latter should then decrease more steeply with increasing E, and thereby eventually cross the γ – E trace for the hex phase.[20]

Based on the presently available evidence, however, we favor another interpretation. The voltammetric data (e.g. Fig. 2 above) show that the hex reconstruction is lifted sharply by about 0.6 V vs SCE in perchloric acid electrolyte, even for moderate or rapid positive-going potential sweeps (< 0.1 V s^{-1}) where diffusion-controlled adsorption of contaminant chloride is unlikely to be significant. Moreover, the C_d – E data used to generate γ – E traces by using the above assumptions are at least as susceptible to the effects of contaminant chloride adsorption. We obtain similar γ – E curves to those given in Fig. 11 of ref. 20 by using C_d – E data obtained in our laboratories. Such a schematic γ – E diagram for the (1 × 1) and hex phases in 10 mM $HClO_4$ is given in Fig. 9. The E_{pzc} values are taken as 0.05 V and 0.25 V, respectively (cf ref. 20); the γ – E curves are arranged to intersect at 0.4 V, as suggested by the observed slow onset of the hex → (1 × 1) transition at nearby potentials (0.35–0.45 V). In order to achieve an intersection of the hex and (1 × 1) γ – E plots by, say 0.4–0.6 V, it is necessary to assume that the γ_{max} values for these surface phases are markedly (ca 5–10 fold) less dissimilar than calculated in ref. 21, so that $\Delta\gamma_{max}$ ~ 20 to 30 dyne cm^{-1} (Fig. 9). If the larger $\Delta\gamma$ estimate (ca 200 dyne cm^{-1}) is maintained, intersection of the γ – E curves by 0.6 V or so requires the presumption of C_d values for the (1 × 1) surface, ca 150 μF cm^{-2}, that are much larger than those observed experimentally, 30–50 μF cm^{-2}, over the

relevant potential range, 0 to 0.6 V.[3,8c,8d]

One is therefore obliged to conclude that the differences in surface free energy between the hex and (1 × 1) phases are small, < 100 dyne cm^{-1} (i.e. < 0.05 eV), throughout the polarizable potential region of interest in perchloric acid, −0.4 to 0.8 V (Fig. 9). (This deduction does not change significantly if the γ–E crossover potential is taken anywhere within the region, 0 to 0.4 V, where the equilibrium potential for the hex ⇌ (1 × 1) transition should be situated.) This smaller energy difference than calculated for the clean Au(100) surfaces in ref. 21 may arise from the stabilizing influence of the double-layer solvent, which should markedly depress the γ values below that of the corresponding metal-vacuum interface, but perhaps to a greater extent on the (1 × 1) surface due to stronger interaction with the aqueous solvent.

Microscopic Mechanisms of Reconstruction Formation

Of central interest here is the utilization of the STM data to deduce likely atomic-level mechanisms which can account for the remarkable potential-induced phase transitions observed on Au(100). A key question is the manner in which the large-scale mass transfer necessary for the occurrence of the partly reversible ⇌ (1 × 1) transition can be driven by the ostensibly small (< 0.05 eV) free-energy differences that characterize this overall process at the Au(100)–aqueous interface in the absence of strong anion adsorption. We consider first the various processes associated with the development of the ordered hex domains from the unreconstructed surface.

The data summarized in Figs. 5 and 6 indicate the presence of two general, yet distinct, mechanisms triggering the initial growth of the ordered hex phase. For the former, illustrated in Fig. 5, the major source of the 24% additional atoms required for hex phase formation is the clusters residing on the ordered

(1 × 1) terraces. The initial formation of the hexagonal close-packed structures, seen as narrow strings (Fig. 5B), involves chiefly mass transport of gold atoms from nearby clusters. This process can be envisaged as involving three distinguishable steps: (1) detachment of gold adatoms from clusters, (2) diffusion of adatoms on the terrace, (3) nucleation and growth of ordered hex strings. Some information on the relative rates of steps (1) and (2) has been obtained from the kinetics of isolated cluster dissipation on Au(111) in air.[22] These experiments indicate that adatom detachment, rather than surface diffusion, is rate determining. While this conclusion may not apply generally, one might expect that step (1) would commonly involve a higher activation energy than (2).

A key issue in the present context is the manner in which the adatoms, once formed, are able to diffuse and then agglomerate into well-ordered hexagonal strings that can extend out to substantial ($\lesssim$ 20–30 nm) distances away from the cluster "sources." There are no direct measurements of gold adatom diffusion rates on (1 × 1) Au(100) terraces. Nevertheless, recent theoretical calculations of surface self diffusion[23] suggest that the so-called "exchange-diffusion" mechanism, recently observed on Pt(100) and Ir(100) by field ion microscopy,[24,25] should also predominate on Au(100). While reliable estimates of the self-diffusion coefficient, D_s, on unreconstructed Au(100) are absent (vide infra), perhaps a lower limit is provided by the measured value on Pt(100), 1.5×10^{-11} $cm^2\ s^{-1}$ at room temperature.[24]

The exchange-diffusion mechanism involves an adatom in a fourfold hollow site submerging into the substrate top-layer lattice and thereby displacing one of the nearest-neighbor atoms. A related, although more concerted, atomic motion can also provide a viable mechanism accounting for the nucleation and growth of the hex strands. This suggested mechanism is shown schematically in Fig. 10.

A pair of adjacent adatoms, shown in initially fourfold hollow sites close to the top of the top-view terrace in Fig. 10A, are envisaged as becoming partly submerged into the (100) lattice. This motion can be accommodated by a commensurate diagonal shift of the nearest-neighbor gold lattice atoms, as indicated. While the energetics of such a concerted motion would appear to be unfavorable when involving only one or two adatoms, the subsequent motion of additional adatoms so to "unzip" the (1 × 1) terrace in one dimension, and form a straight row parallel to the substrate direction, will yield the locally hexagonal-packed arrangement shown in B. The propagation as well as nucleation of this arrangement will clearly be facilitated by the presence of a locally high concentration of gold adatoms (or groups of adatoms as depicted in A).

This simplified "terrace-unzipping" nucleation-growth model can account for the key features of the real-space terrace reconstruction dynamics as observed by STM (Fig. 5). The initial preferential appearance of the strings seen in the vicinity of the clusters, together with the rapid propagation of these strands across extended distances, are nicely consistent with this model. Indeed, the atomic-resolution STM image in Fig. 6, showing an apparently 3-atom wide "pencil" of atoms in a raised hexagonal array, corresponds accurately to the ball-model structure in Fig. 10B. A variety of other structures, related to yet distinct from Fig. 10B, are also observed. Thus the registry between the "overlayer" and surrounding "substrate" lattice can be altered by shifting the former along the y-direction in Fig. 10B. Such structural mutations will affect the relative height of the atoms across the string, accounting for the variations in the observed z-corrugations noted above. Some compression of the adatom rows are commonly observed, judging from the observed z-corrugations in this direction.

The model structure given in Fig. 10B can also provide a reasonable precursor to the wider hexagonal strings that are observed to form in Fig. 5.

Ideally, adding parallel additional adatom rows separated by five substrate atomic spacings (14.5 Å) would generate the characteristic (5 × n) unit cell. The immediate formation of such extended structures would clearly be favored by their continuously interlocked hexagonal packing, but would require that sufficient gold adatoms are available locally. The latter factor can account for the observed tendency of broader hex strings to form in the vicinity of the cluster adatom sources. On the other hand, the observed sudden formation of hex strings, even in isolated terrace regions, argues for the nucleation step being at least partly rate determining.

The role of adatom diffusion in influencing the type of hex structure produced, as well as the formation dynamics, is evident more clearly in the "atomically thin" strands which are prevalent immediately upon stepping from 0 to −0.3 V (Fig. 5D). Presuming for a moment that the formation rate of these strings is limited by adatom diffusion across the (1 × 1) terrace, the observed real-space/-time morphology of the STM image allows us to estimate that $D_s \approx 1 \times 10^{-12}$ cm^2 s^{-1}. (This estimate is derived by noting that the isolated strings are separated on average by ca 100 Å, and can be formed within 1 s after stepping the potential, allowing D_s to be extracted from $(D_s t)^{\frac{1}{2}} = d$, where d ~ 100 Å.) In all likelihood, however, this rapid initial growth of these "single-adatom" strands is limited instead by the availability of terrace adatoms. For this latter circumstance, we can roughly estimate the adatom coverage, θ_a, from the ratio of the areas occupied by the strands and the (1 × 1) terraces. This exercise yields $\theta_a \sim 0.02$. Further development of these strands, as seen in Figs. 5E and F, ultimately (after ca 20 min) yielding a densely interlocking hex phase, is a clearly slower process, involving further detachment of adatoms from clusters and terrace edges.

Another intriguing question concerns the marked acceleration of the

reconstruction dynamics observed from 0 to -0.3 V, given that the free-energy driving force for the overall (1 × 1) → hex phase transition would not appear to increase substantially over this potential range (Fig. 9). A rationalization is that the kinetics of the microscopic rate-limiting step(s) for this process are not necessarily related straightforwardly to the free-energy difference for the overall macroscopic phase change. Thus the initial "terrace unzipping" nucleation step may well be rate controlling, and sensitive to surface charge. It is worth noting that the (1 × 1) surface charge density approaches zero at 0 V vs SCE ($E_{pzc} \simeq 0.05$ V), but is significantly negative (ca 0.05 e^-/surface atom) by -0.3 V. This raises the interesting possibility that the nucleation sites involve "trapped" electronic charge, perhaps localized (at least transiently) by double-layer cations. Indeed, triggering reconstruction by charged sites involving cationic adsorbates has been identified previously by STM, specifically for the potassium-induced reconstruction of Cu(110) *in vacuum*.[30]

In addition to adatom mass transport, the data in Fig. 7 indicate that *concerted* atomic motion can play a role, at least near terrace edges. A schematic picture of a "concerted wavefront" mechanism that can account for these results is given in Fig. 11. The atomic rows at the (1 × 1) terrace edge are envisaged as transforming into a hexagonal pattern with their nearest neighbors, yielding a compressed row. Thus this hexagonal string (not unlike that in Fig. 10) can move as a wavefront away from the terrace edge, as seen in Fig. 7. As before, these strings can combine to form two-dimensional domains of the hex phase.

Lifting of Reconstruction

By comparison with the rates at which the reconstruction forms in weakly adsorbing electrolytes, the kinetics for the hex → (1 × 1) transition under

voltammetric conditions are extremely rapid. Indeed, Skoluda and Kolb found in conventional electrochemical (potential-step) experiments that the relaxation time for this process is as short as 1-2 msec at about 0.6 V in sulfate-containing electrolyte.[13] From the potentiodynamic STM measurements shown in Figs. 3 and 4, the overall process is complete within at least ca 0.5 s as the potential is swept through the voltammetric peak C_p (Fig. 2). As a consequence, the constituent steps leading to the formation of the clusters from the hex domains cannot directly be resolved temporally by STM. Some insight concerning the likely mechanism can nonetheless be gleaned from the data. Thus the observed lifting of larger hex domains at significantly higher voltammetric potentials suggests that the nucleation sites contributing preferentially to this process tend to be formed close to domain edges. This inference is consistent with the expectation that the hex structure will be less stable within these regions. The sequence of images obtained during the slow lifting of reconstruction that occurs at lower potentials (Fig. 8) indicate additionally that removal of the excess gold atoms occurs chiefly at the ends, rather than the sides, of the extended hex strands.

The physical nature of the nucleation sites within the hex phase is unclear. The occurrence of anion specific adsorption would appear to play a role,[4,13] perhaps by aiding the removal of one or more terrace adatoms, most likely top-layer atoms situated at atop sites with respect to the underlying square-planar substrate (Fig. 3 of ref. 8b). The nearby terrace atoms can relax into the less densely packed (1 × 1) structure. Once this relaxation process is started, it is expected to lower the energy barrier for removing additional hex terrace atoms nearby, hence triggering a nucleation-growth process leading to rapid dissipation of the hex domain.

Also instructive is the morphology of the ensuing clusters. The average

distance between the clusters, d_c, enables a lower limit to the gold self-diffusion coefficient to be established under these conditions, given that the clusters appear rapidly (within 1 s) upon lifting the reconstruction. Roughly, $(D_s t)^{\frac{1}{2}} > d_c$; since d_c is 50 Å and 100 Å in perchloric acid and sulfuric acid electrolytes (Fig. 3D and 4B, respectively), then D_s is greater than 2×10^{-13} and 1×10^{-12} cm^2 s^{-1} in these two media (cf limiting D_s estimate for forming hex domains noted above.) However, these limiting D_s estimates may in part refer to the motion of smaller aggregates, formed initially, into the larger clusters seen in the STM images: the actual D_s values for adatom motion are probably markedly larger (cf D_s estimate from hex domain formation.)

A few comments are appropriate here regarding the potential dependence of the reconstruction kinetics. A notable feature is the strong sensitivity of the rate for lifting the reconstruction to the electrode potential. Thus the hex domains are stable almost indefinitely at, say, 0.3 V in perchloric acid, but are lifted within a few minutes at 0.4 V, and < 1 s by 0.6 V. This observation is surprising given the weak potential dependence of the overall hex → (1 × 1) thermodynamics (Fig. 9). While a qualitative explanation can be offered in terms of the potential-dependent appearance of nucleation sites, triggered perhaps by anion adsorption,[4,13] the phenomenon remains ill-understood.

The lower limiting estimates of D_s for gold adatom diffusion on the Au(100)-(1 × 1) terrace obtained here, $\gtrsim 10^{-12}$ cm^2 s^{-1}, is consistent with the experimental value for Pt(100) noted above, but much ($\gtrsim 10^2$ fold) larger than the estimates reported for comparable electrolytes and potentials on polycrystalline gold.[28] The latter measurements, however, refer to the long-range relaxation of surface roughness, and are therefore liable to be dominated by a complex interplay of mass transport across grain boundaries, dislocations, etc. Nonetheless, the D_s values deduced in the manner are seen to increase markedly

(by ca $10-10^2$ fold) in the presence of moderate or strong anion adsorption.[28] Such observations are consistent with the larger D_s estimates deduced above for reconstruction lifting in sulfate versus perchlorate media, and can also account for the dramatically enhanced reconstruction dynamics observed in iodide electrolytes.[16] Such anion effects upon the adatom mobility can be rationalized most simply in terms of a diminution in the activation barrier caused by coordination between the partially charged metal adatom and the inner-layer anions.

Concluding Remarks

The foregoing results highlight a key, yet previously unexploited, virtue of STM applied to electrochemical systems in that one can explore in remarkable detail the real-space dynamics of microscopic phase transitions driven by suitable alterations in the electrode potential. In suitable cases, a wealth of insight concerning the likely mechanisms of surface reconstruction and the attendant mass transport dynamics over distance scales down to atomic dimensions can be obtained, along with the likely density of terrace adatoms utilized in the $(1 \times 1) \rightleftharpoons$ hex phase transition. The potentiodynamic STM technique can readily be applied to the examination of a variety of potential-driven phase transitions involving nonmetallic adlayers as well as metal reconstruction.[15,29] A particularly useful tactic, noted above, is the acquisition of simultaneous potentiodynamic STM and voltammetric data. These two sets of information are naturally complementary in that they refer to local microscopic and averaged macroscopic scales, respectively.

This point is exemplified above in the observation of a significant dependence of the potential at which the hex $\rightarrow (1 \times 1)$ transition occurs on the hex domain size. Besides accounting for the observed voltammetric peak widths,

the microscopic data thereby provide important insight into the nature of the ensemble distributions that together constitute the macroscopic dynamical and structural phenomena. The inherently local nature of the STM probe also lends itself well to the examination of the nucleation–growth phenomena associated with the (1 × 1) → hex transition. In particular, the morphology as well as the growth kinetic of the narrow hex strings seen in the early stages of hex domain growth yield interesting clues as to the nature of the surface mass transport required for development of the reconstruction. While the formation of extensive hex domains is a relatively slow process in nonadsorbing media such as perchloric acid, the use of potential steps during image acquisition provides useful information on the more rapid genesis of domain growth.

Overall, then, while still in their infancy such potentiodynamic STM tactics should contribute increasingly and significantly not only to the current development of a deeper atomic-level appreciation of surface electrochemical phenomena, but also to surface science in a broader perspective.

Acknowledgment

This work is supported by the Office of Naval Research and the National Science Foundation.

References

1) For a review see: M.A. Van Hove, S.-W. Wang, D.F. Ogletree and G.A. Somorjai, Adv. Quantum Chem., 20 (1989) 1.

2) For a recent overview, see: (a) D.M. Kolb, in "Frontiers of Electrochemistry", Vol 2, J. Lupkowski, P.N. Ross, Jr., VCH Publishers, New York, 1993; (b) M.J. Weaver and X. Gao, Ann. Rev. Phys. Chem, in press.

3) (a) A. Hamelin, J. Electroanal. Chem., 142 (1982) 299; (b) A. Hamelin, J. Electroanal. Chem., 255 (1988) 281.

4) (a) D.M. Kolb, J. Schneider, Electrochim. Acta, 31 (1986) 929; (b) Kolb, D.M., J. Schneider, Surf. Sci., 162 (1985) 764; (c) J. Schneider, D.M. Kolb, Surf. Sci., 193 (1988) 579; (d) M.S. Zei, G. Lehmpfuhl, D.M. Kolb, Surf. Sci., 221 (1989) 23.

5) (a) A. Friedrich, B. Pettinger, D.M. Kolb, G. Lüpke, R. Steinhoff, G. Morowsky, Chem. Phys. Lett., 163 (1989) 123; (b) B. Pettinger, J. Lipkowski, S. Mirwald, A. Friedrich, J. Electroanal. Chem., 329 (1992) 289.

6) (a) B.M. Ocko, J. Wang, A. Davenport, H. Isaacs, Phys. Rev. Lett., 65 (1990) 1466; (b) I.M. Tidswell, N.M. Markovic, C.A. Lucas, P.N. Ross, Phys. Rev. B, in press.

7) (a) J. Wang, B.M. Ocko, A.J. Davenport, H.S. Isaacs, Phys. Rev. B, 46 (1992) 10321; (b) B.M. Ocko, G. Helgensen, B. Schardt, J. Wang, A. Hamelin, Phys. Rev. Lett., 69 (1992) 3350.

8) (a) X. Gao, A. Hamelin, M.J. Weaver, Phys. Rev. Lett., 67 (1991) 618; (b) X. Gao, A. Hamelin, M.J. Weaver, Phys. Rev. B, 46 (1992) 7096; (c) A. Hamelin, X. Gao, M.J. Weaver, J. Electroanal. Chem., 323 (1992) 361; (d) A. Hamelin, L. Stoicoviciu, G. Edens, X. Gao, M.J. Weaver, J. Electroanal. Chem., submitted.

9) X. Gao, A. Hamelin, M.J. Weaver, J. Chem. Phys. 95 (1991) 6993; (b) X. Gao, A. Hamelin, M.J. Weaver, Phys. Rev. B, 44 (1991) 10983; (c) X. Gao, M. J. Weaver, Ber. Bunsenge. Phys. Chem., 97 (1993), 507.

10) (a) N.J. Tao, S.M. Lindsay, J. Appl. Phys., 70 (1991) 5141; (b) N.J. Tao, S.M. Lindsay, Surf. Sci., 274 (1992) L546.

11) (a) J. Hotlos, O.M. Magnusson, R.J. Behm, N. Batina, D.M. Kolb, to be published; (b) O.M. Magnusson, J. Wiechers, R.J. Behm, Surf. Sci., in press.

12) For example: (a) M.A. Van Hove, R.J. Koestner, P.C. Stair, J.P. Biberian, L.L. Kesmodel, I. Bartos, G.A. Somorjai, Surf. Sci., 103 (1981) 189; (b) K.H. Rieder, T. Engel, R.H. Swendsen, M. Manninen, Surf. Sci., 127 (1983) 223; (c) Y.-F. Liew, G.-C. Wang, Surf. Sci., 227 (1990) 190; (d) S.G.J. Mochrie, D.M. Zehner, B.M. Ocko, D. Gibbs, Phys. Rev. Lett., 64 (1990) 2925.

13) P. Skoluda, D.M. Kolb, Surf. Sci., 260 (1992) 229.

14) X. Gao, M.J. Weaver, J. Am. Chem. Soc., 114, (1992) 8544.

15) X. Gao, G. Edens, M.J. Weaver, in preparation.

16) X. Gao, G. Edens, M.J. Weaver, in preparation.

17) For example: J.D.E. McIntyre, W.F. Peck, Jr., in "The Chemistry and Physics of Electrocatalysis", J.D.E. McIntyre, M.J. Weaver, and E.B. Yeager, eds., Electrochemical Society, Pennington, NJ, 1984, p. 102.

18) A. Hamelin, in "Modern Aspects of Electrochemistry", Vol. 16, B.E. Conway, R.E. White, J. O'M Bockris, eds., Plenum, New York, 1986, p. 1.

19) G.A. Somorjai, M.A. Van Hove, Prog. Surf. Sci., 30 (1989) 201.

20) P.N. Ross, A.T. D'Agostino, Electrochim. Acta, 37 (1992) 615.

21) D. Tomanek, K.H. Bennemann, Surf. Sci., 163 (1985) 503.

22) D.R. Peale, B.H. Cooper, J. Vac. Sci. Tech., A10 (1992) 2210.

23) C.L. Liu, J.M. Cohen, J.B. Adams, A.F. Voter, Surf. Sci., 253 (1991) 334.

24) G.L. Kellogg, Surf. Sci., 246 (1991) 31.

25) C. Chen, T.T. Tsong, Phys. Rev. Lett., 64 (1990) 3147.

26) X. Gao, M.J. Weaver, to be published.

27) For example: (a) G.E. Rhead, Surf. Sci., 47, (1975) 207; (b) J.A. Venable, T. Doust, J.S. Drucker, M. Krishnamurty, "Kinetics of Ordering and Growth at Surfaces", M.G. Lagally, ed., Plenum Press, New York, 1990.

28) (a) J.M. Doña, J. González-Velasco, Surf. Sci., 274 (1992) 205; (b) M.P. Garcia, M.M. Gómez, R.C. Salvarezza, A.J. Arvia, J. Electroanal. Chem., 347 (1993) 237.

29) O.M. Magnussen, J. Hageböck, J. Hotlos, R.J. Behm, Disc. Far. Soc., in press.

30) R. Schuster, J.V. Barth, G. Ertl, and R.J. Behm, Surf. Sci., 247, (1991) L229.

Figure Captions

Figure 1

STM images for Au(100) flame annealed using Method I (see text). A was obtained in air; B was acquired in 0.1 M $HClO_4$ at 0.2 V vs SCE.

Figure 2

Voltammograms obtained at 50 $mV \cdot s^{-1}$ for Au(100) in 10 mM $HClO_4$. Solid trace: initial positive-going sweep for surface prepared by Method I. Dashed trace: for surface prepared using Method II, after holding potential at −0.35 V for 6 min. Dotted trace: subsequent voltammogram, obtained immediately after potential excursion to 0.8 V.

Figure 3

A–C) Sequence of potentiodynamic STM images, gathered for surfaces prepared by Method I in 0.1 M $HClO_4$ during initial 10 $mV \cdot s^{-1}$ positive-going potential sweep from −0.2 V showing lifting of reconstruction (see text). D) Similar example as in B, but for surface prepared by Method II.

Figure 4

Similarly to Figure 3, but for surface prepared by Method II in 0.1 M H_2SO_4.

Figure 5

Sequence of STM images for surface prepared by Method II, in 0.1 M H_2SO_4. A) Immediately after stepping potential from 0.6 to 0 V. B) 5 min later. C) 10 min after B. D) Upon altering potential from 0 to −0.3 V (see text). E) 20s after completing D. F) 5 min after D.

Figure 6

Atomic-resolution STM images of example of narrow ("3-atom") hexagonal string on (1 × 1) terrace.

Figure 7

Sequence of STM images for surface prepared by Method II, in 0.1 M $HClO_4$, showing development of "wavefront" motion away from terrace edge (see text).

Figure 8

Sequence of STM images, recorded at 2 min intervals at 0.4 V, showing slow dispersal of hex reconstructed domains.

Figure 9

Schematic plot of surface tension versus electrode potential for hex and (1 × 1) phases of Au(100) surface in perchloric acid electrolyte (see text).

Figure 10

Atomic ball model, displaying suggested "terrace unzipping" mechanism for Au(100) reconstruction.

Figure 11

Schematic picture of suggested "concerted wavefront" mechanism for Au(100) reconstruction.

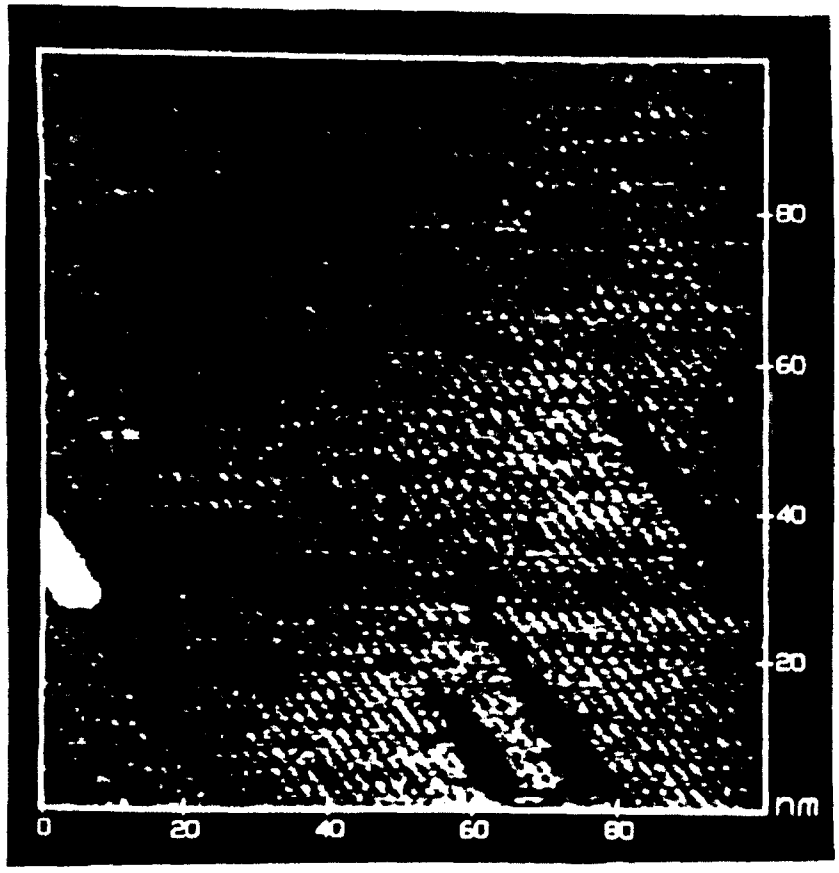

A

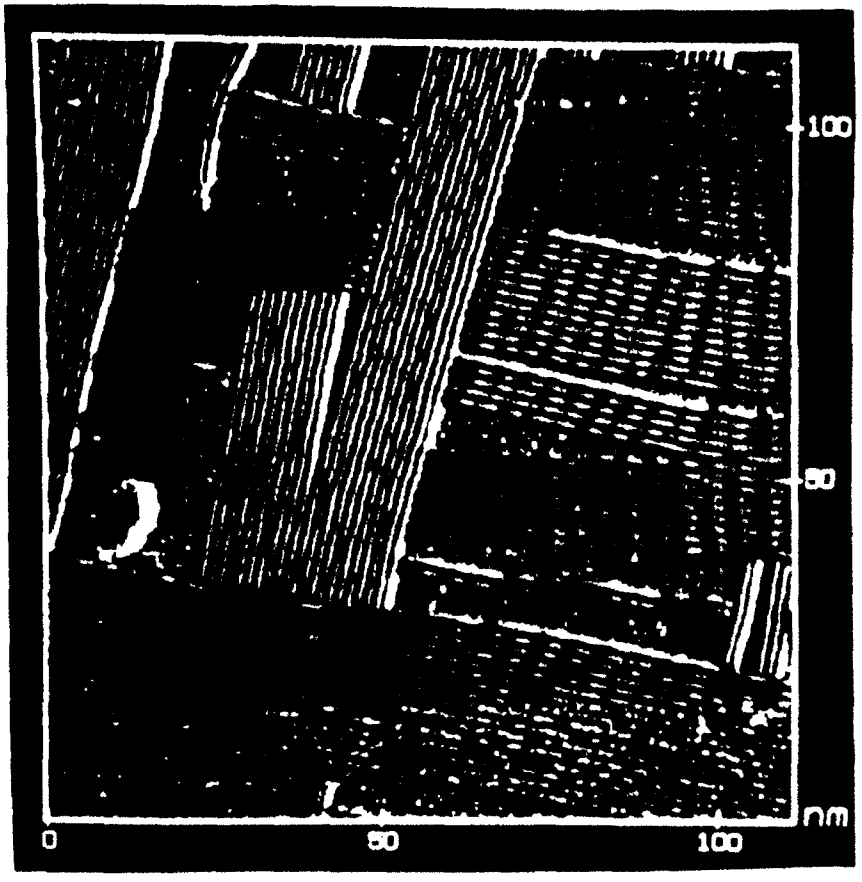

B

FIG 1

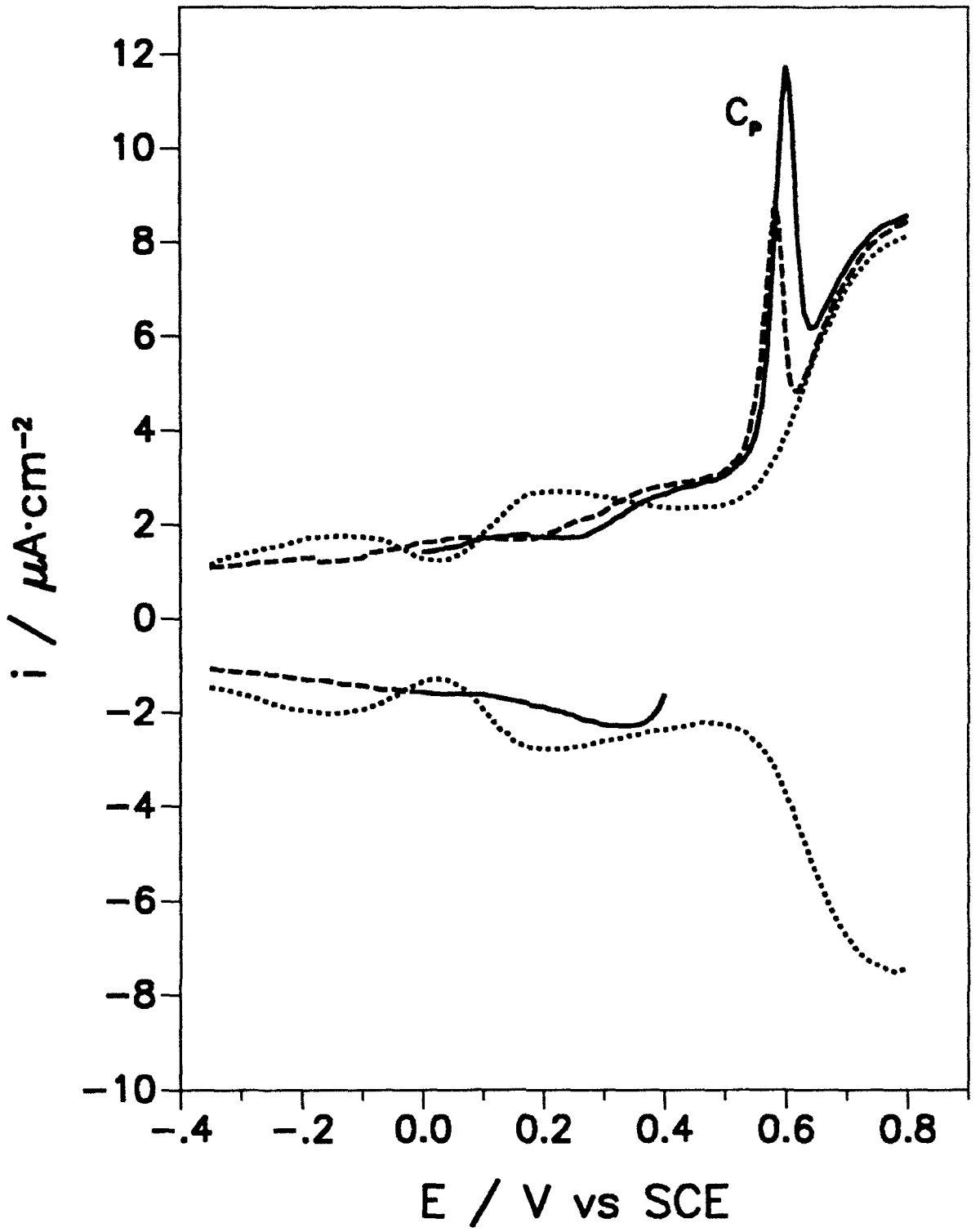

FIG 2

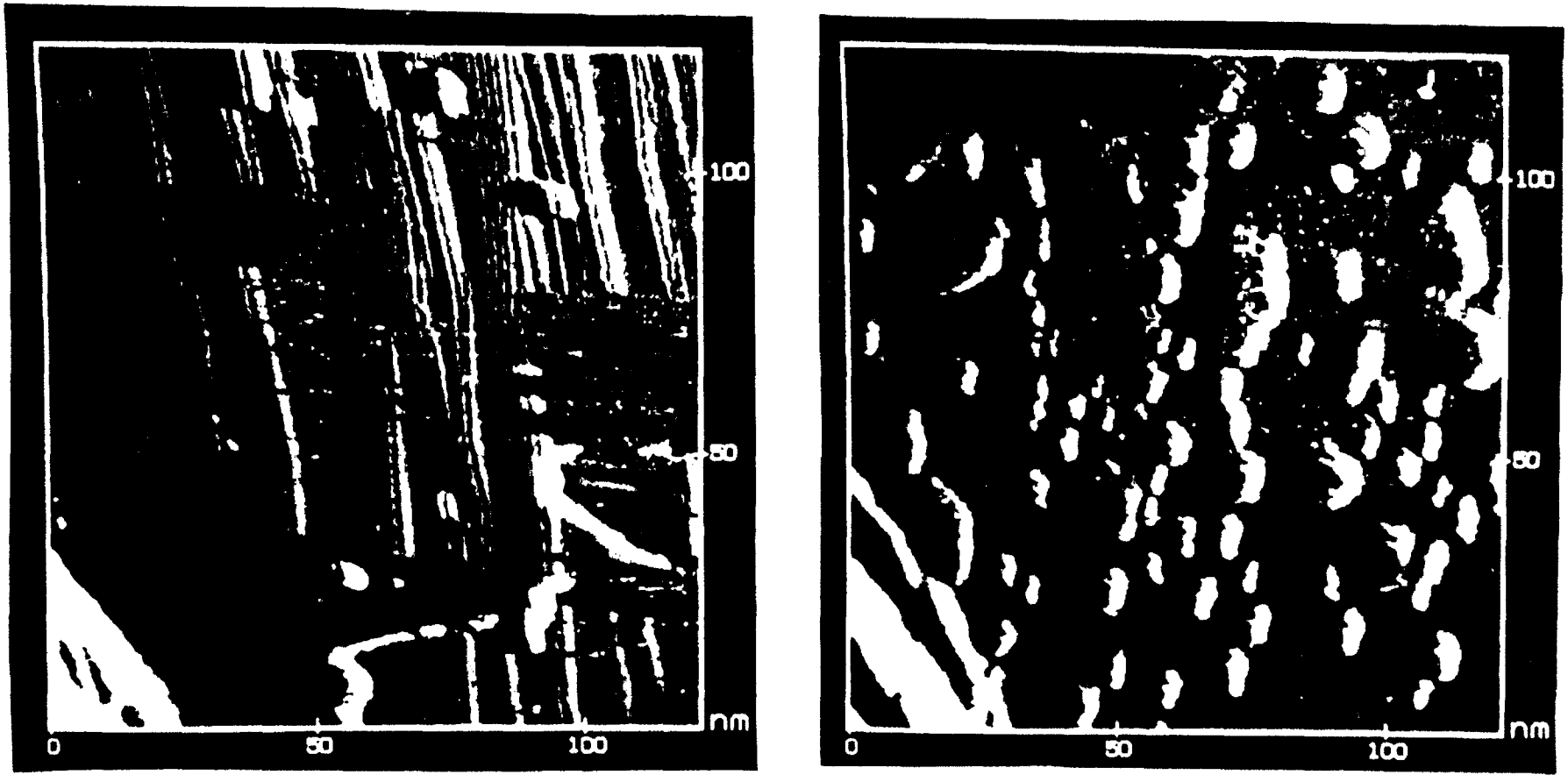

A

B

FIG 3

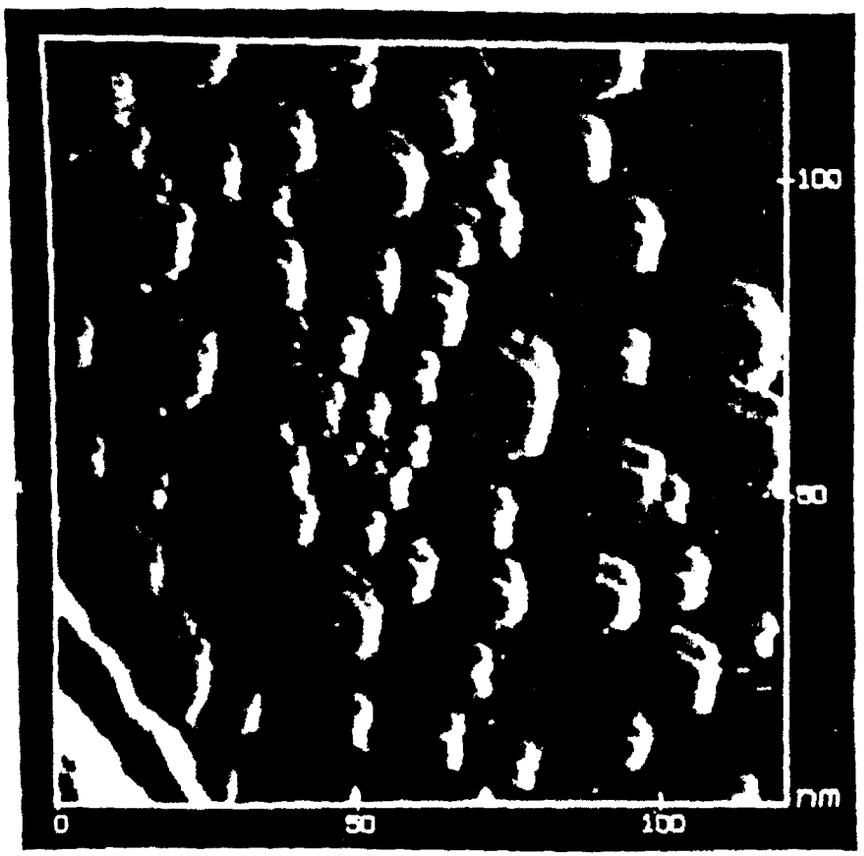

C

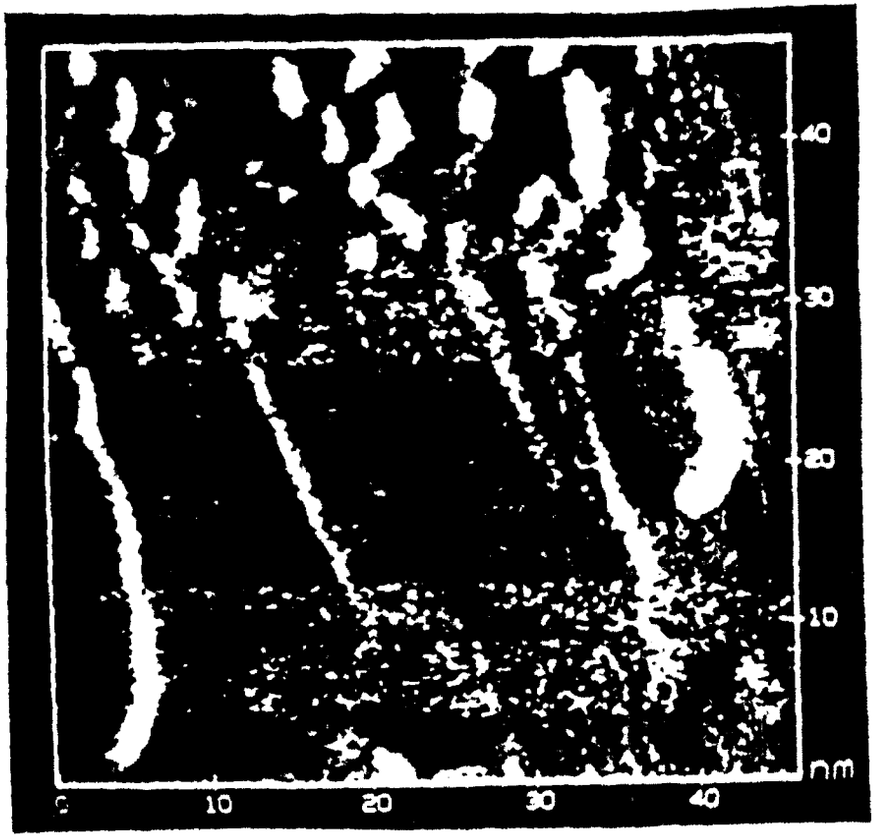

D

FIG 3 (CONTD)

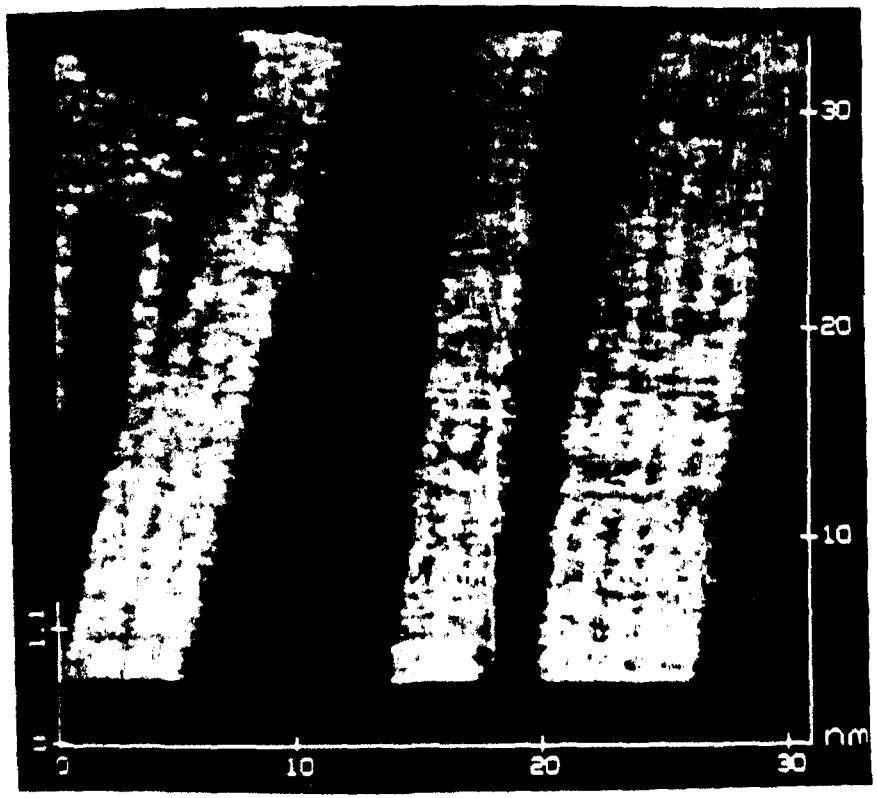

A

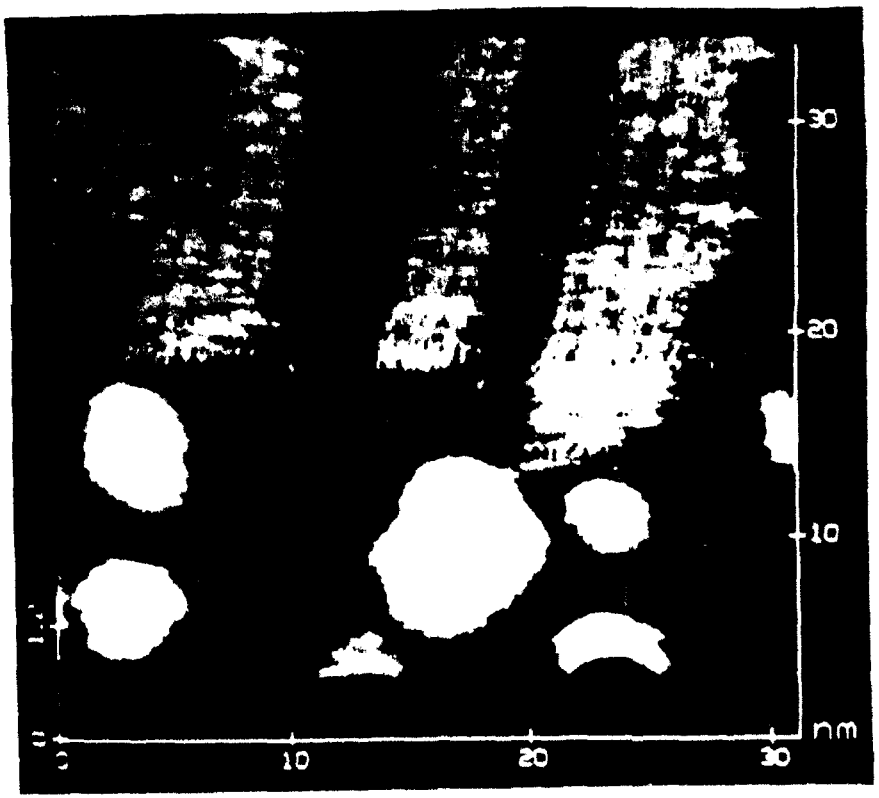

B

FIG 4

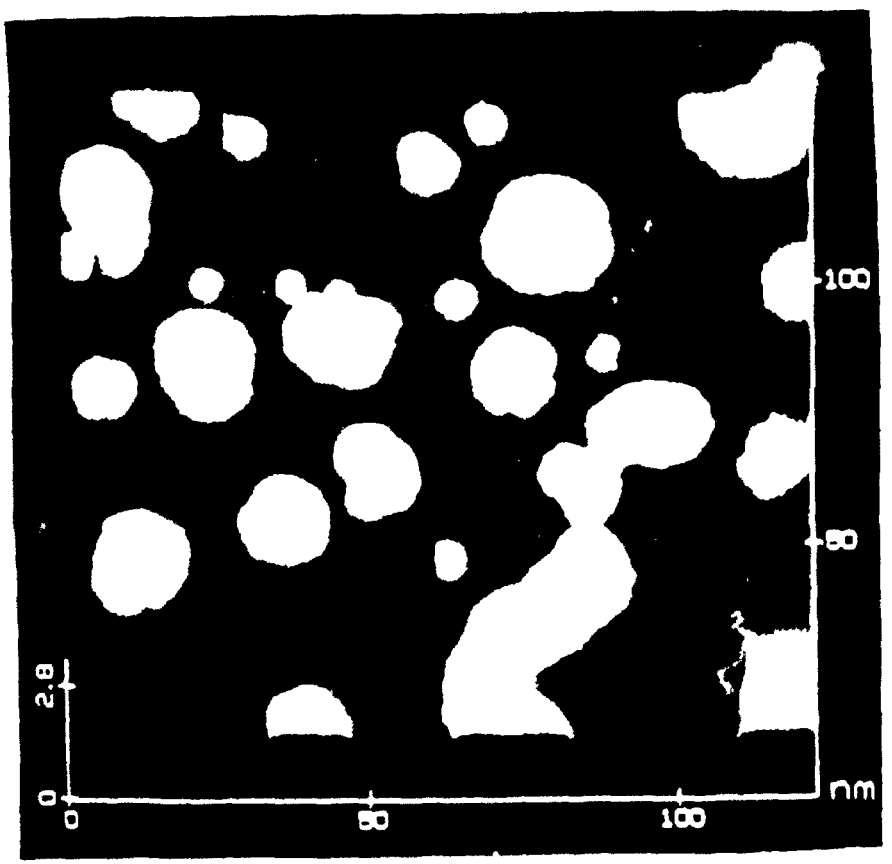

A

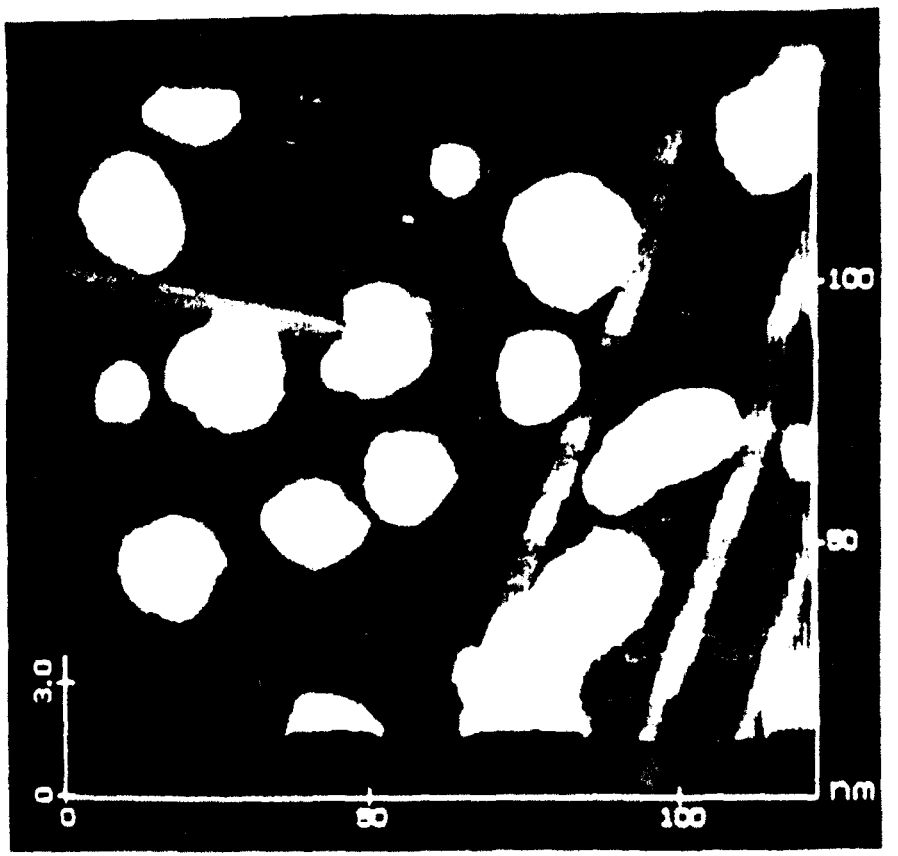

B

FIG 5

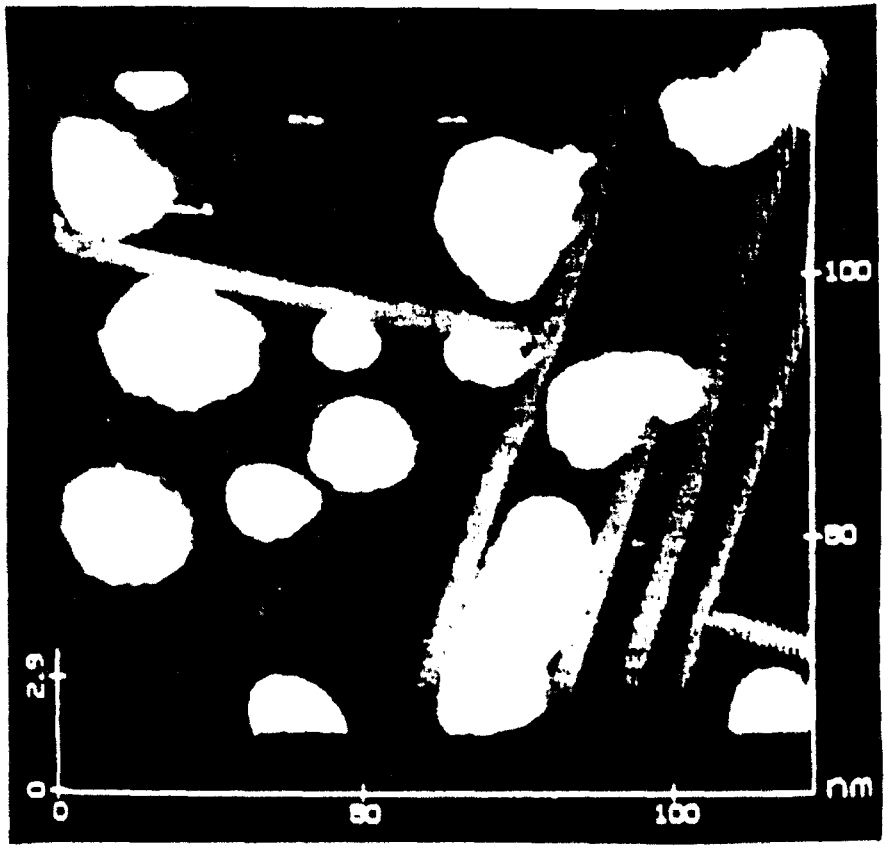

C

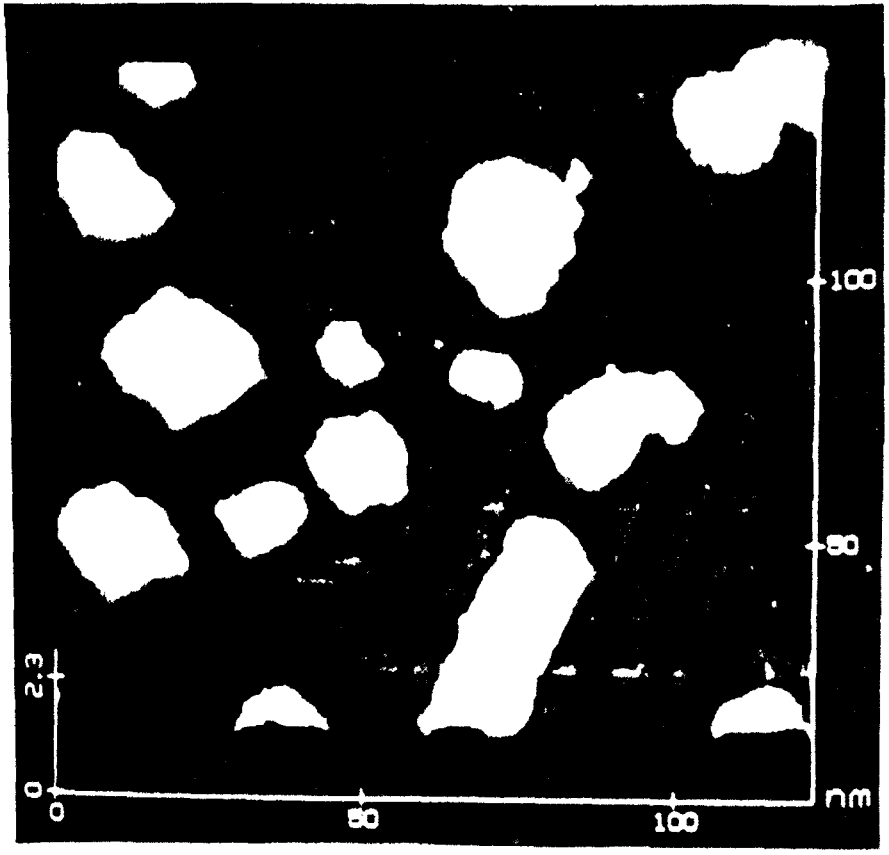

D

FIG 5 (CONTD.)

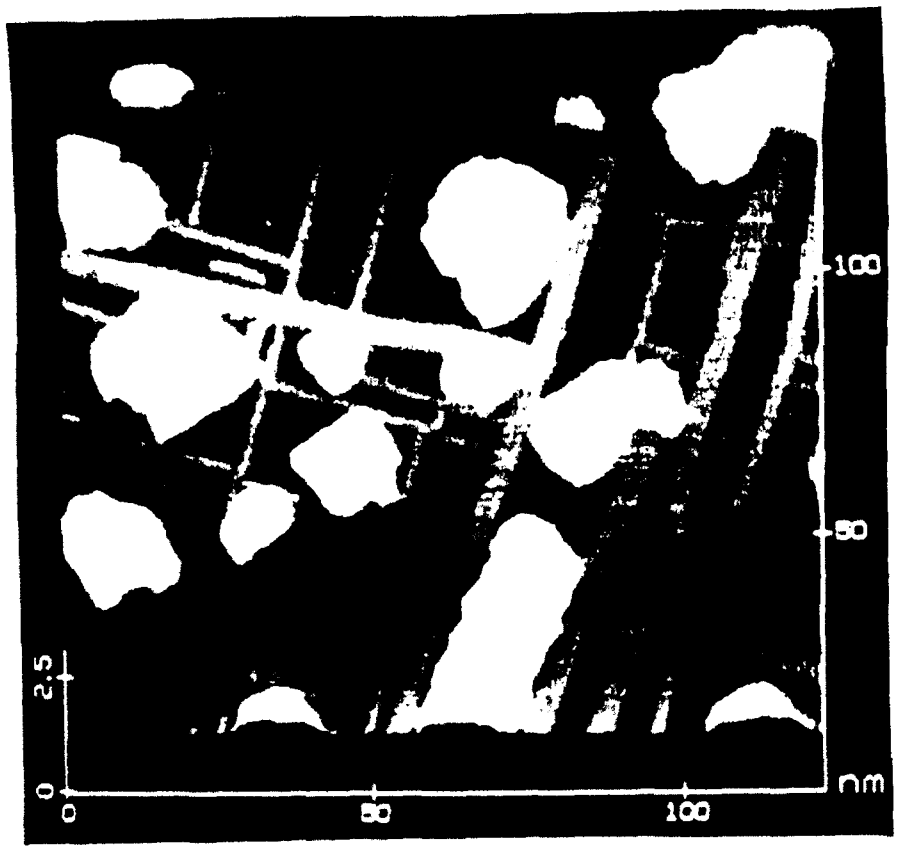

E

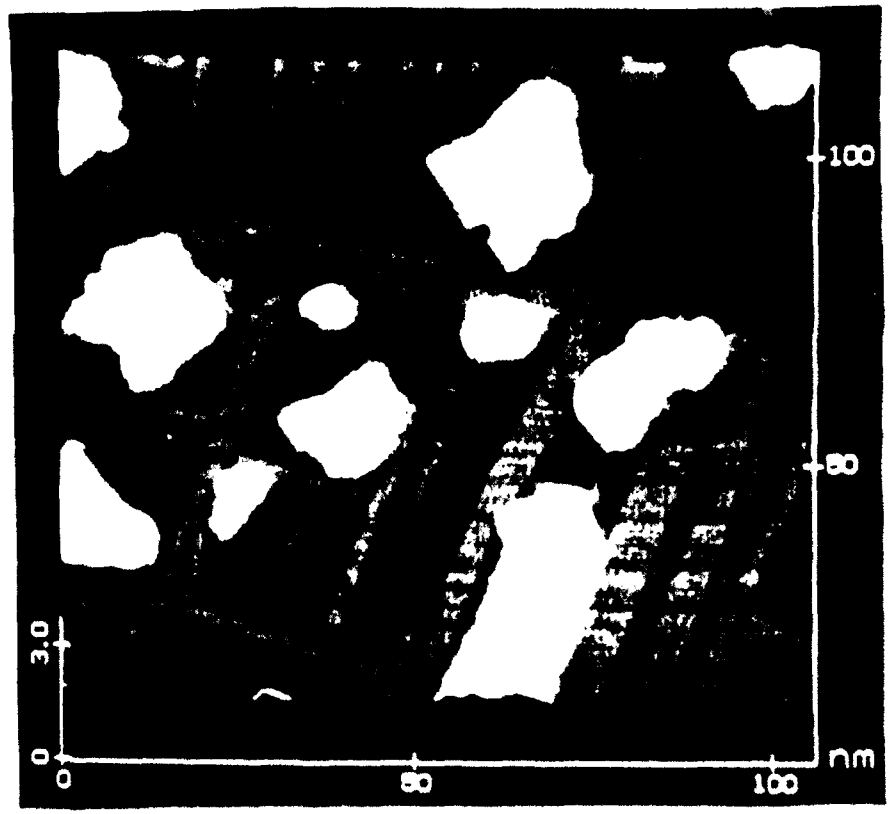

F

FIG 5 (CONTD.)

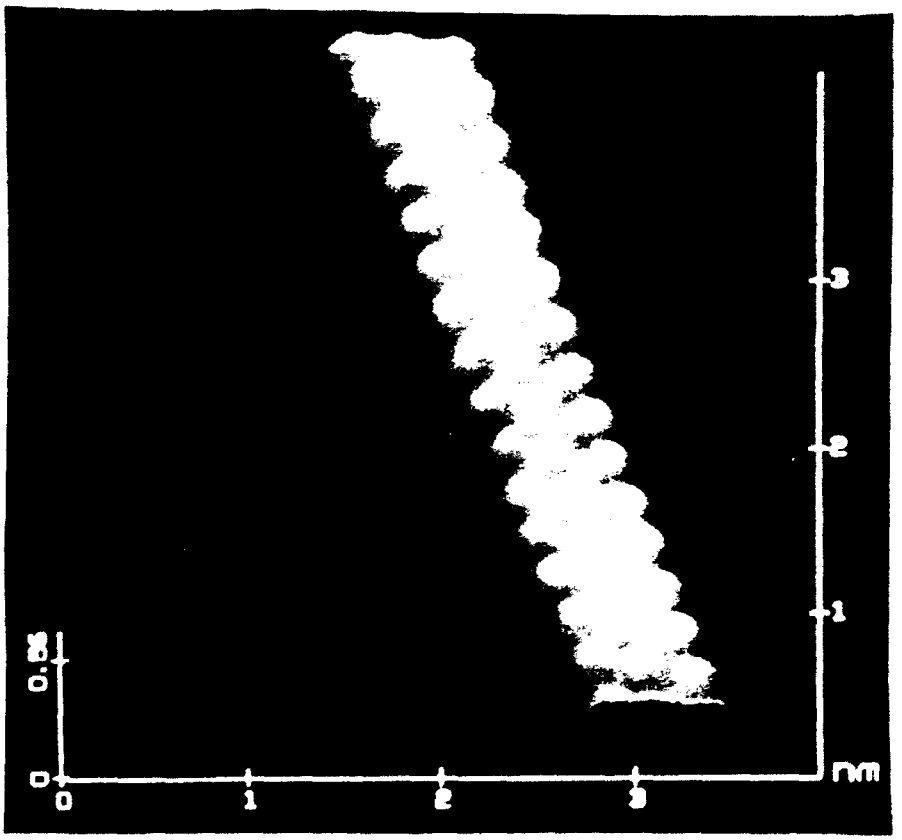

FIG 6

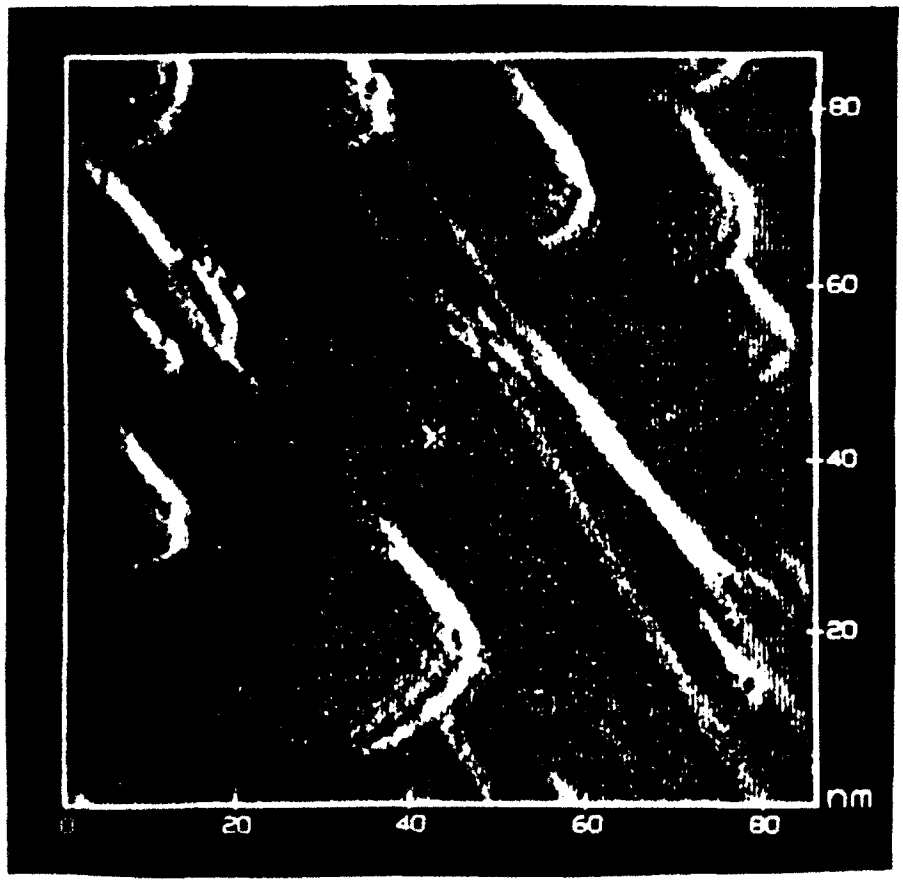

A

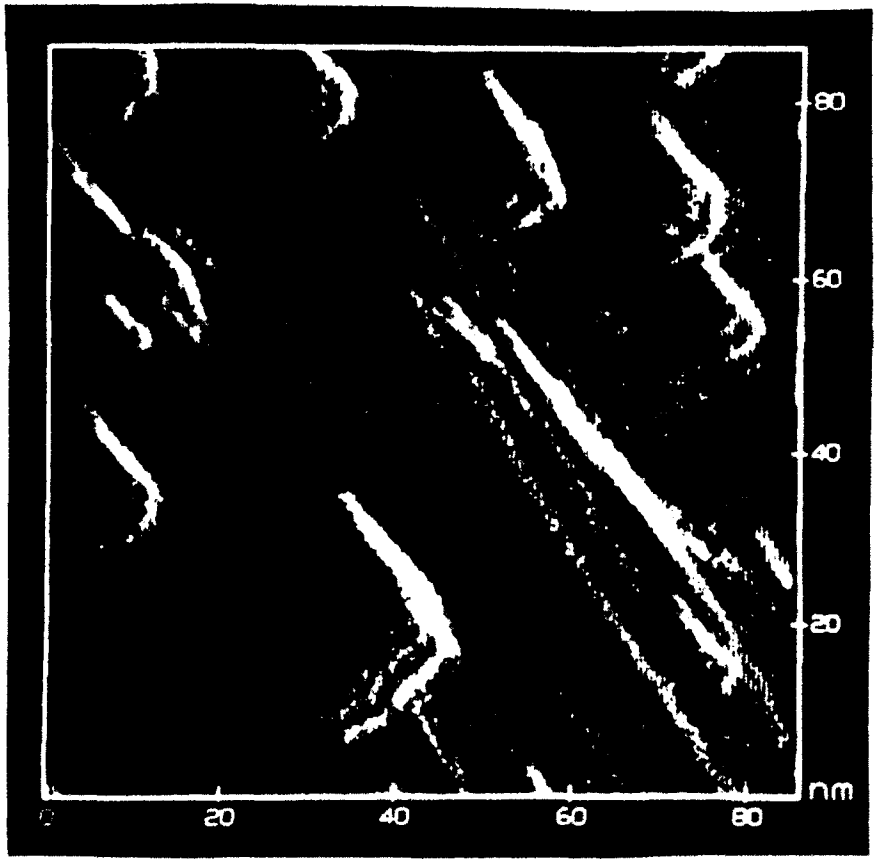

B

FIG 7

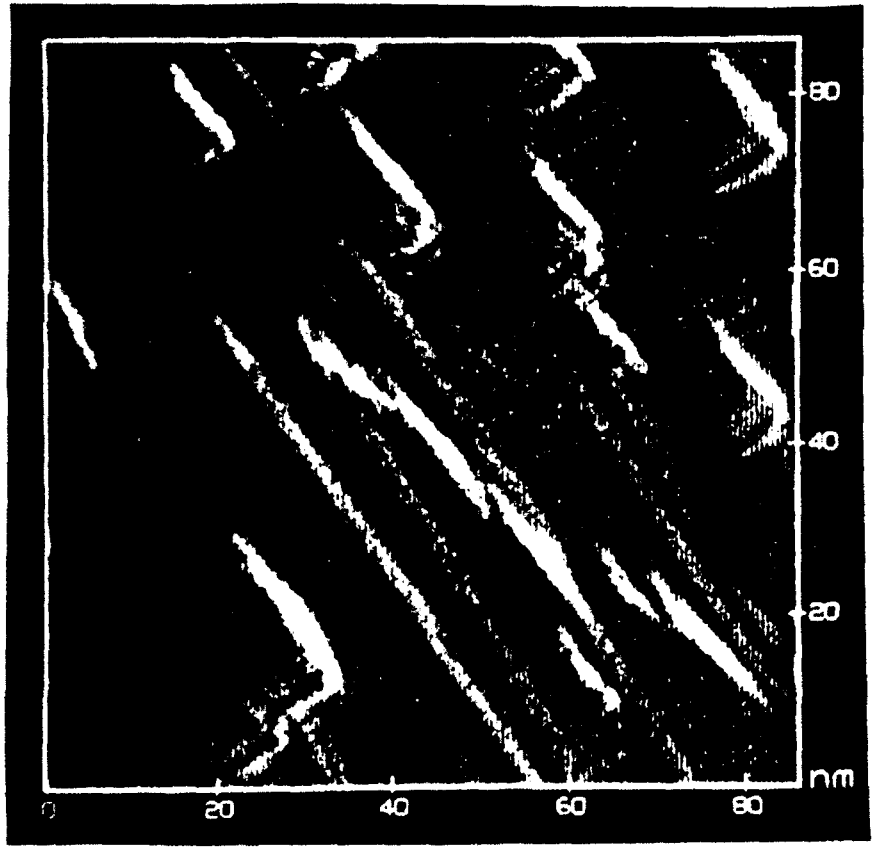

C

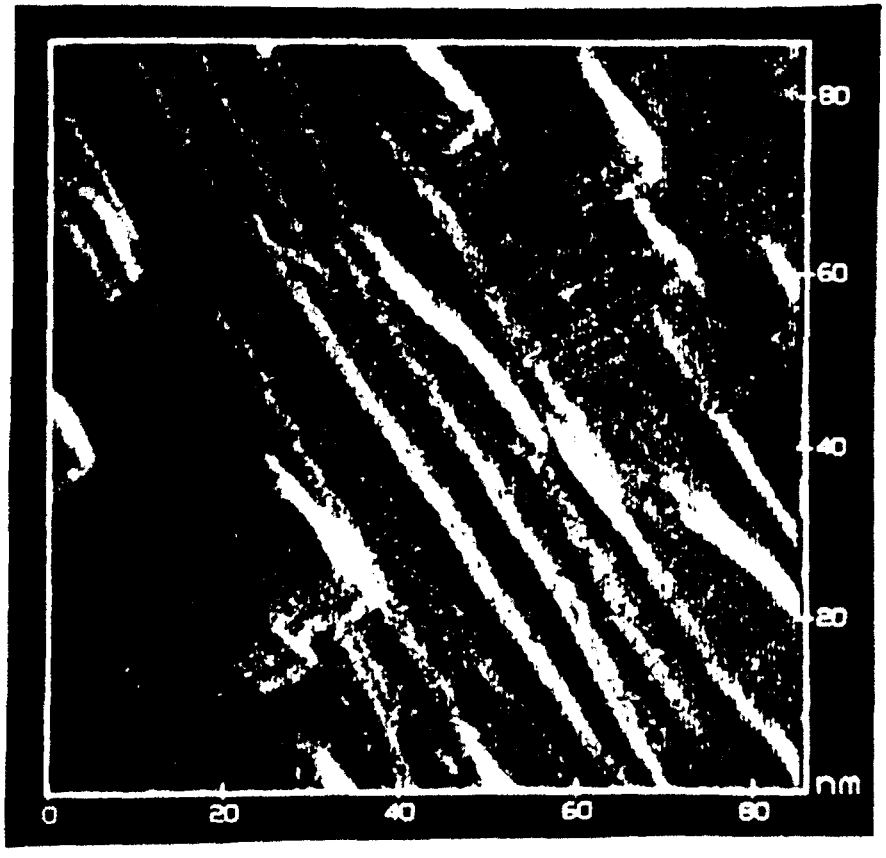

D

FIG 7 (CONTD.)

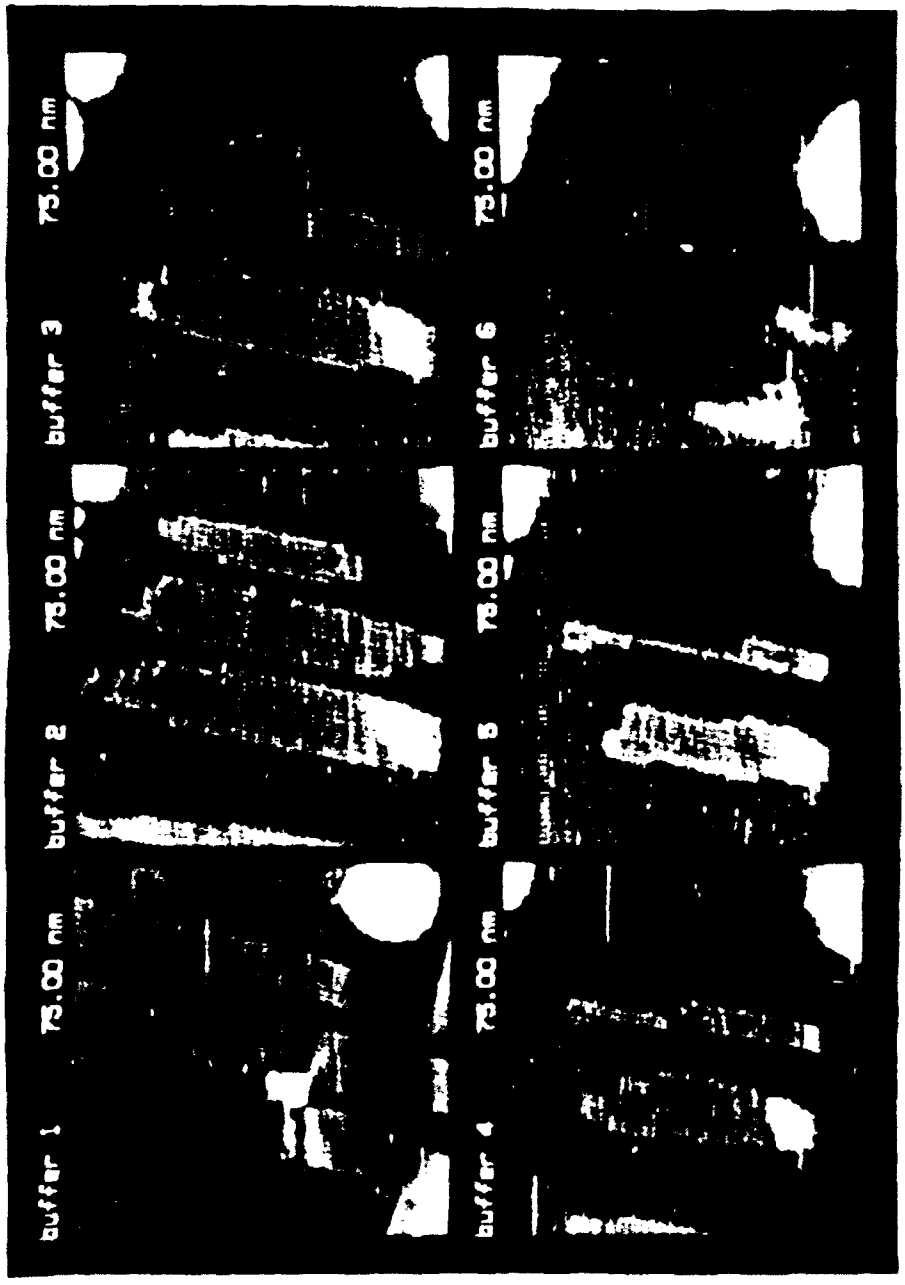
buffer 1
75.8 nm
buffer 2
75.8 nm
buffer 3
75.8 nm
buffer 4
75.8 nm
buffer 5
75.8 nm
buffer 6
75.8 nm

FIG 8

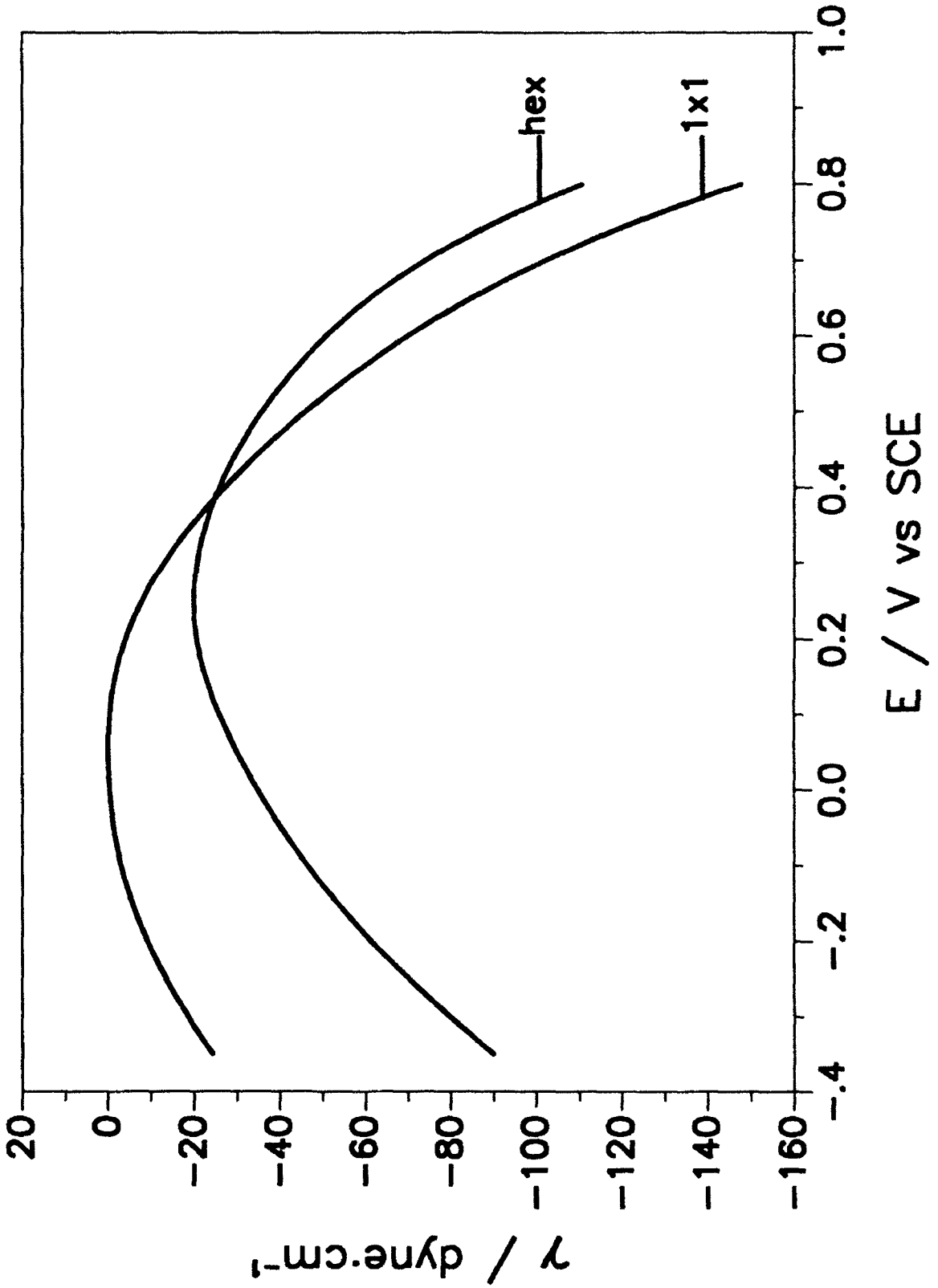
hex
1x1
20
0
−20
−40
−60
−80
−100
−120
−140
−160
−.4
−.2
0.0
0.2
0.4
0.6
0.8
1.0
γ / dyne.cm⁻¹
E / V vs SCE

FIG 9

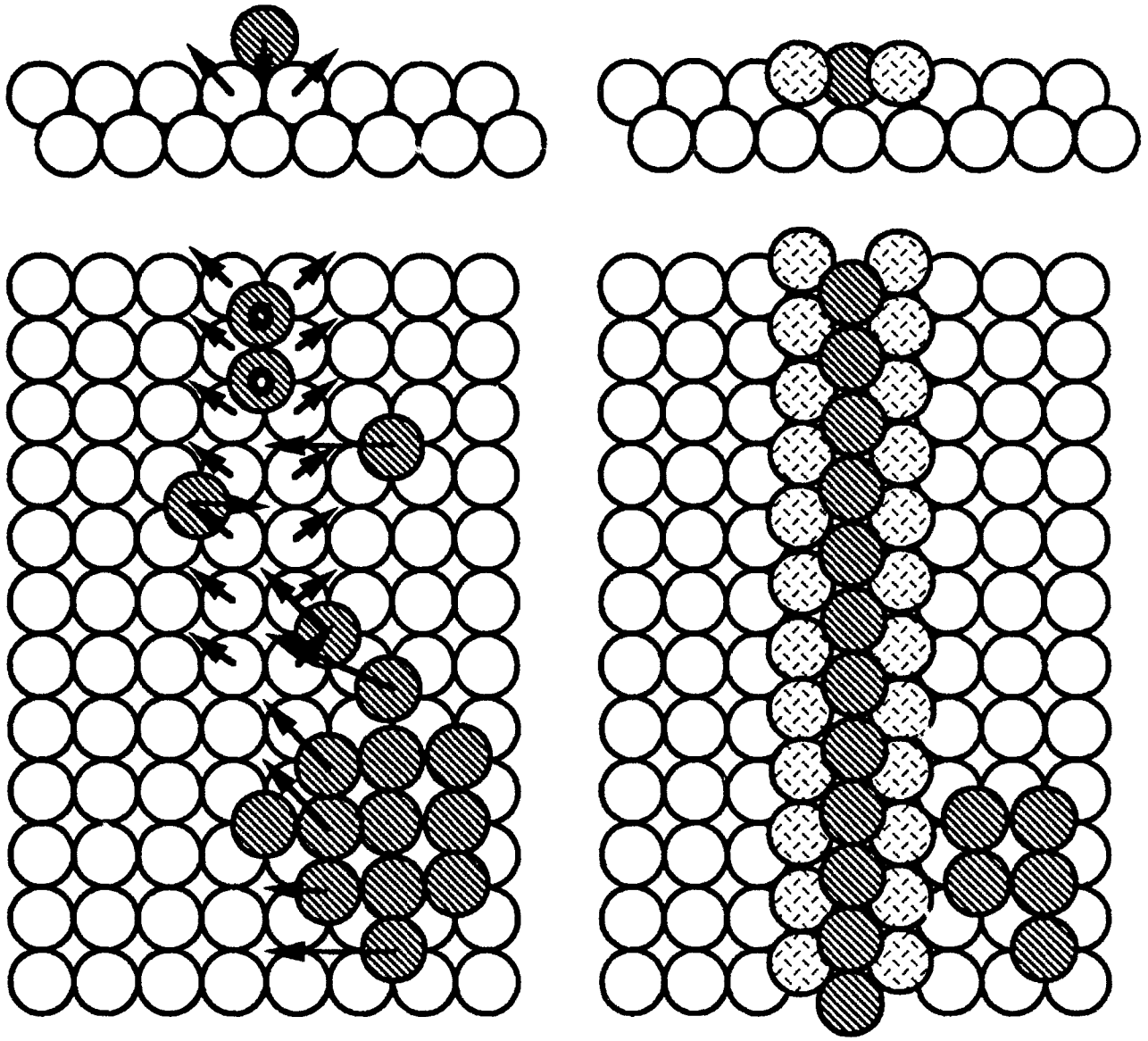

Au(100) reconstruction mechanism I: "terrace unzipping "

FIG 10

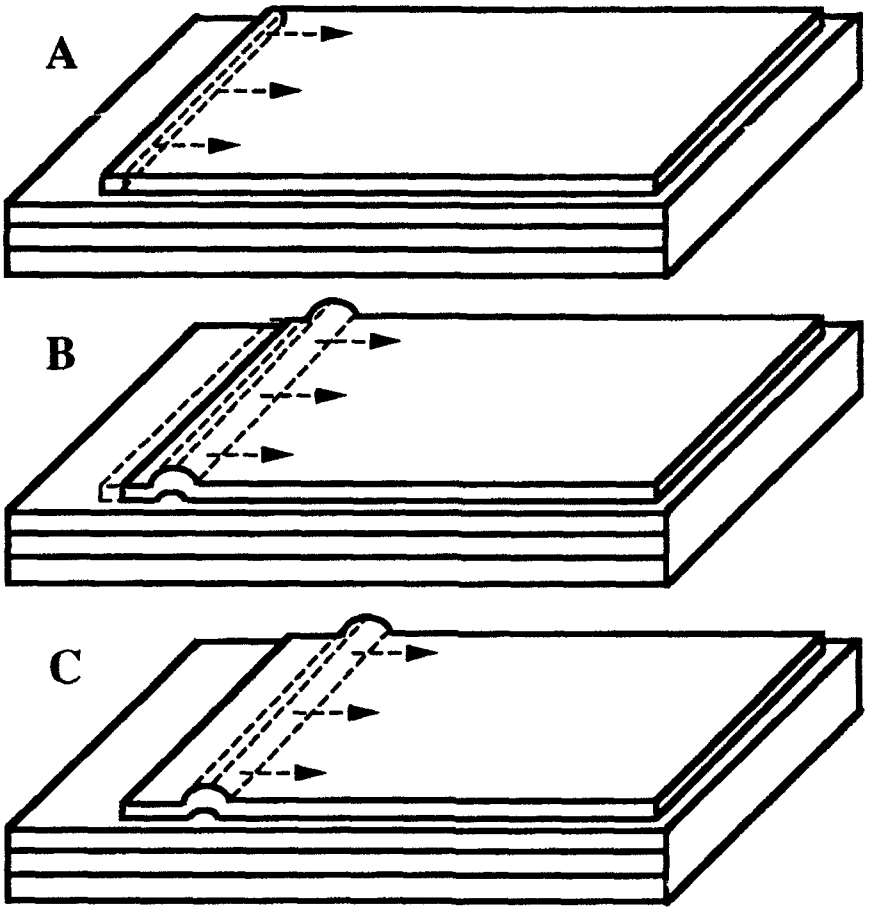

Au(100) reconstruction mechanism II: wavefront motion

FIG 11